NASA/CR—2017–219428

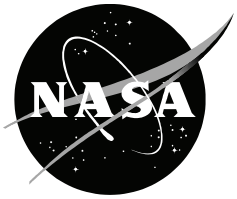

Measurement and Modeling of Multicopter UAS Rotor Blade Deflections in Hover

Nathalie Nowicki
KTH Royal Institute of Technology
Ames Research Center, Moffett Field, California

June 2017

NASA STI Program ... in Profile

Since its founding, NASA has been dedicated to the advancement of aeronautics and space science. The NASA scientific and technical information (STI) program plays a key part in helping NASA maintain this important role.

The NASA STI program operates under the auspices of the Agency Chief Information Officer. It collects, organizes, provides for archiving, and disseminates NASA's STI. The NASA STI program provides access to the NTRS Registered and its public interface, the NASA Technical Reports Server, thus providing one of the largest collections of aeronautical and space science STI in the world. Results are published in both non-NASA channels and by NASA in the NASA STI Report Series, which includes the following report types:

- TECHNICAL PUBLICATION. Reports of completed research or a major significant phase of research that present the results of NASA Programs and include extensive data or theoretical analysis. Includes compilations of significant scientific and technical data and information deemed to be of continuing reference value. NASA counterpart of peer-reviewed formal professional papers but has less stringent limitations on manuscript length and extent of graphic presentations.

- TECHNICAL MEMORANDUM. Scientific and technical findings that are preliminary or of specialized interest, e.g., quick release reports, working papers, and bibliographies that contain minimal annotation. Does not contain extensive analysis.

- CONTRACTOR REPORT. Scientific and technical findings by NASA-sponsored contractors and grantees.

- CONFERENCE PUBLICATION. Collected papers from scientific and technical conferences, symposia, seminars, or other meetings sponsored or co-sponsored by NASA.

- SPECIAL PUBLICATION. Scientific, technical, or historical information from NASA programs, projects, and missions, often concerned with subjects having substantial public interest.

- TECHNICAL TRANSLATION. English-language translations of foreign scientific and technical material pertinent to NASA's mission.

Specialized services also include organizing and publishing research results, distributing specialized research announcements and feeds, providing information desk and personal search support, and enabling data exchange services.

For more information about the NASA STI program, see the following:

- Access the NASA STI program home page at http://www.sti.nasa.gov

- E-mail your question to help@sti.nasa.gov

- Phone the NASA STI Information Desk at 757-864-9658

- Write to:
  NASA STI Information Desk
  Mail Stop 148
  NASA Langley Research Center
  Hampton, VA 23681-2199

NASA/CR—2017–219428

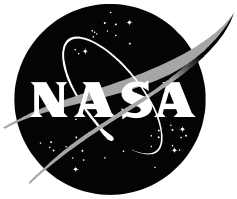

Measurement and Modeling of Multicopter UAS Rotor Blade Deflections in Hover

Nathalie Nowicki
KTH Royal Institute of Technology
Ames Research Center, Moffett Field, California

National Aeronautics and
Space Administration

Ames Research Center
Moffett Field, CA 94035-1000

June 2017

Acknowledgments

First and foremost, I would like to thank my mentor Carl Russell at the NASA Ames Rotorcraft Aeromechanics Branch for all the assistance, guidance, and discussions throughout this project. Without him showing me and providing help on how to set up measurements, especially all the electronic parts, I would not have been able to complete this project. I am also grateful for all of the things that I got to learn thanks to this project.

I would likewise like to thank Dr. William Warmbrodt, without whom I would not have had the internship at NASA Ames or the possibility of writing this thesis at the Rotorcraft Aeromechanics Branch. His encouragement, energy, and enthusiasm in every aspect of the internship—from the work we did to all the extra tours and California history lessons he gave—are admirable, and I am grateful for having had the chance to work for such an inspiring person. Furthermore, I want to thank him for opening my eyes to the field of rotorcraft, and many interesting topics and problems that still need solving.

Next I would like to acknowledge my mentor and examiner at KTH, Per Wennhage, for giving me support and answering all my questions whenever needed, even though I was far away. I would also like to thank the staff at KTH Lightweight Structure Laboratory for taking time and showing me how to use the equipment I needed for my material tests.

Lastly I would like to say a thank you to the staff and interns at the Rotorcraft Aeromechanics branch for making my stay at Ames so memorable. I had great support from many people who took their time to explain and show things that were new to me, without whom I would not have learned as much as I did.

Table of Contents

Table of Contents (cont.)

List of Figures

List of Figures (cont)

List of Tables

Nomenclature

A – rotor disc area [m^2]

α_0 – angle of attack at zero lift [rad]

β – blade flapping angle [rad]

β_0– blade coning angle [rad]

β_p– blade pre-coning angle [rad]

c – blade chord length [m]

C_d – drag coefficient

C_l –lift coefficient

$C_{l\alpha}$ – slope of lift vs. angle-of-attack curve

C_T – thrust coefficient

dD – section drag [N/m]

dL – section lift [N/m]

ϕ – pitch angle [rad]

γ – lock number

I_b– mass moment of inertia about flap hinge [kg m^2]

K_β – torsional spring stiffness constant [Nm]

λ – rotor inflow ratio

m – mass per unit length [kg/m]

μ – mean value

N – total number of samples

N_b – number of blades on rotor

ν – nondimensional flap frequency

Ω – angular frequency of rotor [rad/s]

R – radius of rotor, total blade span [m]

ρ – density [kg/m^3]

s_μ – standard error of the mean

σ – rotor solidity

T – rotor thrust [N]

θ – blade pitch angle [rad]

Nomenclature (cont.)

U – inflow velocity [m/s]

U_p – perpendicular component of inflow velocity [m/s]

U_T – tangential component of inflow velocity [m/s]

x_i – measured value in statistical sample

y – spanwise coordinate from center of rotation [m]

Subscripts

$.8$ – value at 80 percent blade span

NFP – value at no flapping plane

tw – linear twist rate

y – spanwise coordinate

Abbreviations

ABS – Acrylonitrile Butadiene Styrene

ARC – Ames Research Center

BDAS – Basic Data Acquisition System

BEM – Blade Element Momentum

CAD – Computer Aided Design

CAMRAD – Comprehensive Analytical Model of Rotorcraft Aerodynamics and Dynamics

CFD – Computational Fluid Dynamics

CFRP – Carbon Fiber Reinforced Plastic

DSLR – Digital Single-Lens Reflex

DSP – Digital Speckle Photography

EASA – European Aviation Safety Agency

FAA – Federal Aviation Administration

FE – Finite Element

FEA – Finite Element Analysis

FFT – Fast Fourier Transform

KTH – KTH Royal Institute of Technology

RPM – Revolutions per Minute

Nomenclature (concluded)

TTL – Transistor–Transistor Logic

UAS – Unmanned Aerial System

UAV – Unmanned Aerial Vehicle

VABS – Variational Asymptotic Beam Sectional

MEASUREMENT AND MODELING OF MULTICOPTER UAS ROTOR BLADE DEFLECTIONS IN HOVER

Nathalie Nowicki[1]

Ames Research Center

Summary

Package deliveries, surveillance, and entertainment are all areas of a growing market for unmanned aerial systems (UAS). Multicopters, being one of the most popular UAS, can both be bought and built rather easily due to their fairly simple design and low cost. However, a lack of regulations and an absence of research of structural properties of the rotor blades motivated this project, as better knowledge results in safer products with an increased operational envelope.

The out-of-plane deflection and the change in pitch of two commercially available multicopter UAS rotor blades, one plastic and one carbon fiber reinforced, were studied for an isolated rotor in hover mode. The deformation was measured using both a Digital Single-Lens Reflex (DSLR) camera and tailored photogrammetry with two cameras for a rotation speed range. The results were compared to analytical expressions of the coning angle from helicopter theory and to a model developed for a finite element simulation. The conclusion is that for the plastic blades, the out-of-plane deflection is negative quadratic to linear in relation to the rotational speed, while the pitch has a trend of decreasing angle. For the carbon fiber blades, the relation is more linear to quadratic for the deflection, while the pitch is almost constant.

1. Introduction

Multicopters are becoming one of the more common and popular types of unmanned aerial systems (UAS) that have both civilian and military applications. One example of the civilian application of UAS is the concept of drone deliveries proposed by the distribution company Amazon [1]. The use of such electrical propulsion systems is considered to result in faster and easier deliveries. There are also environmental benefits compared to other vehicles that still use fossil fuels. Additionally, there is the benefit of reduced complexity and increased reliability compared to traditional internal combustion engines. Other application examples include surveillance and entertainment. The reason behind UAS success is often said to be due to their small size, relatively low cost, simple structure, and simple usage.

With an increase in the UAS market comes challenges in terms of security, as both people and other aircraft could be harmed if UAS are not used correctly. Therefore further studies and regulations based on these concerns are needed to ensure that the future use of drones, especially in the civilian and public sectors, is safe and efficient. Thorough research has been done on full-scale (meaning man or cargo transporting) helicopters such that most parts of flight and performance are fairly well understood. However, much of the flight and performance data has not been verified for small multicopters. Until recently, there has also not been much research done on control systems and navigation, and even less has been investigated within the fields of aerodynamics and structures. Many of the methods used today for

[1] KTH Royal Institute of Technology, Department of Lightweight Structures, Stockholm, Sweden.

building multicopters involve a process of trial and error of what will work well together. Once that is accomplished, some structural analysis of the multicopter bodies might be done to verify that the product will be strong enough and have a decent aerodynamic performance.

Similarly, not much has been done on the research of the rotor blades themselves, especially in terms of structural stress analyses and ways to ensure that the commonly used parts are indeed safe and follow safety measures. Some producers advertise that their propellers have been tested, but again, it usually tends towards simple fluid dynamic analyses or even simpler stress analyses. There is no real deflection measurement of said blades, and today all theory is based on the theory developed for full-scale helicopters. This report intends to highlight the problems that come with blade deflection theory and measurements for small UAS multicopters.

This report starts with the introduction and problem formulation where the ground for the report scope is laid out, followed by a chapter with the history and basic background information of UAS multicopters for readers not familiar with the field. A literature review of the research within the area is then presented, where previous and current research and methods are discussed. The experimental section presents the blade types that were studied and the two methods that were used for the measurements. Relevant theory regarding coning angles is presented to be able to compare the experimental results with theoretical results. A chapter with the computer simulation is then included with the finite element analysis and material analysis. In the results section, the obtained results are presented for the different subparts. Finally, there is a discussion where the results and methods are evaluated and analyzed, followed by the most important conclusions.

1.1 Problem Formulation

The aim of this report is to investigate the deformation of commercially available rotor blades of multicopters during hover, such as quadcopters, by performing measurements of these deformations. Two measuring methods were used; the first using a Digital Single-Lens Reflex (DSLR) camera and the second by using photogrammetry. These results are then compared with theoretical results and analyzed. The second part of the project tried to recreate the measurements in a numerical simulation by using finite element analysis (FEA).

This project is one part of a larger project. The overall goal is to gather data and performance information of multicopter UAS so that a new subpart can be added to the way rotorcraft vehicles are studied at the NASA Ames Research Center (ARC) Rotorcraft Aeromechanics Branch today. By doing so, it will be possible to predict the performance and analyze a new product design in the early stages of development, thus making it possible to not only increase the product's operational envelope, but also to create safety regulations that need to be followed.

1.2 Method

This project was mostly carried out at NASA Ames Research Center (ARC) in Moffett Field, California. The approach to solve the problem contained two distinct parts: one experimental part with measurements performed in the AEROLab at NASA ARC Aeromechanics Branch, and one smaller simulation part where the blade deflections and structural properties were confirmed using FEA. The experimental approach was carried out with two methods of measuring the out-of-plane deflection: one using a DSLR camera and one using tailored photogrammetry.

The simulations were performed using a combination of different software programs, including PTC Creo Parametric 2.0, ANSYS Workbench 16, and Matlab. Due to uncertainties of material properties, tests were performed at the Lightweight Structures Laboratory at KTH Royal Institute of Technology in Stockholm, Sweden. The results from the different methods and simulations were compared, analyzed, and checked for their validity, giving a more thorough and complete explanation of how the blades of commercially available multicopters react to loads associated with hover mode.

1.3 Limitations

Since the project was carried out during an internship, the generation of data from experiments was done in a limited time frame and limited to the resources of the department where it was conducted. Therefore, not all desired data could be gathered and the photogrammetry method could not be improved. The time limitation also meant that only one FEA model was tested and evaluated. Another factor was the author's limited background in fluid dynamics, and hence no computational fluid dynamics (CFD) analysis was performed to obtain the actual aerodynamic loads for the complete hover simulations. Instead, these loads were approximated from analytical expressions.

2. Background: UAS Multicopters

Rotorcraft are heavier-than-air machines that produce lift by a rotational motion of blades. Unlike a fixed wing vehicle, rotorcraft have one or more rotating hubs with blades attached to them. The rotation induces an airflow over each blade and thus creates lift. The main benefit of vertical lift aircraft is that less infrastructure is needed for landing and takeoff, so there is less environmental impact due to building runways and also easier access to otherwise unreachable places. The most common vertical lift aircraft is the helicopter. However, other vertical lift aircrafts have been developed, such as the tiltrotor aircraft (AgustaWestlands AW609 and Boeing V22 Osprey) that have a tilting rotor providing both a helicopter and airplane mode.

Over the last few years, the development of small multicopters has begun, as unmanned systems have been developed, and new markets have emerged where the system is needed. One such example is the proposed Amazon drone delivery program [1] [2]. The hope for this program is to benefit society through faster, more precise deliveries with less environmental impact. However, if used improperly, the devices could cause harm from accidents with regular air traffic or operation in restricted areas. Thus an increase in regulations for such vehicles might be needed.

A multicopter is an unmanned aerial vehicle (UAV) containing, per definition, more than one rotor. A UAV is part of a UAS, which includes the multicopter and the ground control system, meaning the flying component or UAV is controlled remotely from a separate location. The size of multicopters can range from a couple of centimeters to over a meter depending on the purpose of usage and on how much payload is needed. Today the upper mass limit, including the payload, for a small UAV in the USA is 25 kg, as regulated by the U.S. Federal Aviation Administration (FAA) [3]. However, most of the civilian applications usually have a mass of 1–3 kg and can take as much in payload, depending on the configuration. There is a market need for higher payloads, but there are still many problems that need to be solved before the upper limit of 25 kg can be implemented. These problems include the structural layout of the drones, control systems, lift generation with limited amount of power supply, and safe transport from point A to point B. Before a safe product with a capacity for higher payload can be achieved, the product needs to be studied and better understood so that authorities, such as the FAA and the European Aviation Safety Agency (EASA), can regulate the safety criteria on new products.

2.1 Structure

The most common multicopters today are the quadcopters and octocopters, having 4 and 8 rotors respectively. The structure of a multicopter includes the frame, propulsion system, and communication and navigation systems, as well as the rotors with corresponding propellers. The frame is usually made of some lightweight material such as plastic, aluminum, or fiber composite to reduce the thrust and thus power needed for lift and maneuvering. Multicopter propellers, consisting of a hub and blades, are most often a single rigid piece unlike typical helicopter rotors, resulting in a hingeless rotor structure. Due to the small area and aerodynamic effects such as very low Reynolds numbers, the blades are often highly cambered and twisted. This is once again the opposite of traditional helicopter blades and necessitates using viscous analysis for determining aerodynamic constants. The propeller is often made of a lightweight, yet rather stiff, material such as a polymer plastic or a fiber composite.

Many of the quadcopter propellers that can be bought today are typically either made out of injection molded thermos plastics, such as Nylon 6, or carbon fiber reinforced plastic (CFRP). The latter often has a sandwich structure, meaning the carbon fiber reinforcement is on the outside of a core made out of a lightweight, yet dense, material. One of the blades used in this project was the T-motor 15x5 [4] propeller that has a cork wood core coated with carbon fiber reinforced epoxy. The use of cork wood, in this application, is most likely only for obtaining the proper outer geometry and a light hollow structure. Otherwise, foams and balsa wood are used for many small applications where a sandwich concept is needed for improved stiffness. Nonetheless, a comparative review on cork based materials by Gil [5] claims that several studies have been performed on different cork wood combinations for sandwich structures, showing great mechanical properties.

2.2 Flight

Since the multicopters are a type of rotorcraft, their flight dynamics depend on the blades and configuration of the rotors. In the case of a quadcopter, the four rotors need to produce enough lift force to counteract the weight of the aircraft and its payload, as well as the drag due to the movement of air. The loads acting on the multicopter are the classical aircraft loads such as thrust, drag, weight, and lift. Due to the rotating blades, some parts of the drone will experience torque. Just like in regular helicopters, a torque is produced on the body due to the rotating hub. To counteract the torque of each rotor, two rotors spin clockwise while two spin counterclockwise, thus leading to a zero net torque when in hover, vertical, or forward flight. The most common configuration is to have the rotors spinning in the same direction in a diagonal pattern, as shown in Figure 1.

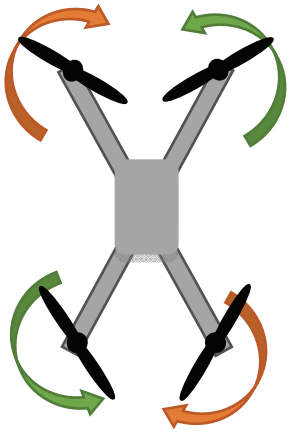

Figure 1: Sketch of a quadcopter with rotation directions defined.

Similar to other rotorcraft, multicopters have several flight modes. These include vertical lift and descent, hover and rotation, and forward and reverse flight as well as banking. These modes depend on how the rotors interact with each other. If all are producing equal thrust and there are no disturbances from outside, the UAV will remain in vertical lift or hover. For a quadcopter, if two of the rotors are spinning faster than the others, it will pitch, roll, or yaw accordingly due to the change in net force direction. The biggest issue with these aircraft is that the motors require a tremendous amount of energy to stay in the equilibrium state of hover. This problem requires any vertical lift aircraft to have much more powerful engines than the vehicle would

need for moving. The hover state is nevertheless a unique and powerful maneuver, as it allows the aircraft to become stationary midair, meaning that operations such as surveillance, loading, and unloading are possible.

3. Literature Review

As mentioned in the introduction, many studies have been done on system controls, navigation, and CFD for UAS multicopters. There are many examples of student degree projects at several universities, as well as projects by academic researchers, where new multicopter prototypes have been built and analyzed in various ways [6] [7] [8] [9] [10]. Throughout these projects, more thorough CFD and structural analysis of the bodies, along with actual flight tests in labs, are usually done once the prototype is built and not when it is still in the design stage. Thus, the methodology for new designs is reliant on prior knowledge and trial and error, rather than actually analyzing the new concept at the design stage. Although blades have not been investigated as thoroughly in the structural domain, some examples can be found that mention the flapping phenomenon. Two such examples include the Ph.D. dissertation by Pereira [11], who studied similar aircraft but focused on the performance of the whole vehicle instead of only the blade structure, and Huang et al. [10], who investigated how the flapping phenomenon affects the aerodynamic loads and control stability of a UAS.

Nonetheless, research within the field is on the way. Brandt and Selig [12] created a propeller performance database where several propellers were studied and analyzed. The authors found that a proper choice of a rotor blade will affect the performance of the whole UAS with respect to thrust and efficiency. Additionally, Russell et al. [13] recently presented a paper on the performance of multicopter UAS vehicles where data was generated both in a wind tunnel simulating forward flight and in hover. This data is used for enhancing design and analysis software for better understanding of said vehicles and is also the predecessor of the study presented herein.

For full-scale helicopters, which require a human pilot inside, numerous tests and simulations have been performed, as well as thorough analytical theories that have been developed throughout the years. Several researchers have contributed to the theory and numerical methods used in analyzing the structure and aeroelastic behavior of rotor blades, both isotropic and those containing anisotropic composite materials. One such investigation was performed by Ormiston and Hodges [14] who studied the linear flap-lag dynamics of hingeless rotors in hover, a field that describes some of the important movements of the rotor blades. Much effort has also been put into developing the anisotropic beam theory for rotor blades. For example Hodges [15], who worked on the nonlinear composite beam theory, also put together a thorough review of composite rotor blade modeling. Additionally, Friedmann and Yuan [16] studied the aeroelasticity and structural optimization of composite rotor blades by using an analytical approach with moderate deflection theory. One of the results of that study pointed to how different composite lamina layups affect parameters such as blade torsion, but not the blade flapping. That theory was later incorporated into dedicated analytical codes.

3.1 Codes for Rotor Blade Analysis

There are several methods that have been implemented into various codes for analyzing new concepts and ideas for helicopters. The hope is that these codes could also be used for analyzing the much smaller multicopter UAS.

For many years, the approach of analyzing rotor blades and hubs has been to perform the aerodynamic simulations and structural analyses separately [17]. This is mainly due to the problem of combining the software, programming, and theory of the two fields. The structural analysis is primarily done with the help of approximated load distributions generated by the aerodynamic studies. The helicopter rotors have always been a complicated mechanism with a complex hub containing many parts and long slender rotor blades that are attached to the hub in various ways, depending on the rotor type. This, along with a complex load case, lead to the use of beam models for analyzing the structural properties of the rotor blades and the hubs. This way, enough simplification can be incorporated in the design to allow solvable analyses without too much computer power and have sufficient fidelity for simple analyses.

One example of this is Sivaneri and Chopra [18], who studied the aeroelastic stability of the flap bending in hover by using beam elements for the FEA and 2D airfoil analysis for the aerodynamic loads. The authors claim that the approach gives reliable results and is simple to implement for analyzing the aeroelastic properties of complex blade geometries. Keep in mind that the focus of the study has been on helicopter hingeless and articulated hubs, and it has not been tested on multicopter blades.

Later on, when the theory was better understood and developed, the two fields were combined in several analyzing codes. An analysis tool that is still used today is the Variational Asymptotic Beam Sectional (VABS) analysis program that decouples a 3D model of, for instance, a blade, into a 1D engineering beam model with the desired cross section that can be analyzed. It can incorporate the different cross-section geometries of the blades and use anisotropic materials. From this, the aerodynamics loads can be determined for a cross section and then through the 1D approximation for the whole blade. According to Hodges and Yu [19], VABS was developed throughout the years and to large content based on Hodge's nonlinear composite beam theory. The program was also used in the authors' study of wind turbines and rotors.

Furthermore, a comparison between different analysis models such as VABS and the theory by Yuan and Friedmann [16] has been done by Freidmann et al. [20]. The authors prove that even though the approach to defamation varies, the moderate deflection composite beam model from Yuan and Friedmann [16] can be incorporated into VABS, which is said to give "a more accurate stress field due to the more general treatment of warping" [20]. The model and its implementation are clearly helpful for analyzing composite rotor blades and make VABS more reliable as well as usable in more applications.

Johnson [21], on the other hand, has created a model and tool called Comprehensive Analytical Model of Rotorcraft Aerodynamics and Dynamics, also known as CAMRADII. The program can use input from, for instance, VABS, to perform the complete rotorcraft analysis with aerodynamic and structural loads, yet the structural model is still based on 1D beam elements. The author claims that the results generated by the code correspond well with the results of large deflections from real life tests, but it has problems with some formulations, hence slightly reducing its fidelity.

These days, anisotropic composites are becoming even more advanced, and new regulations create new design problems. More thorough 3D analyses of the hub and blade structures are desirable in order to analyze a concept with higher fidelity and lower cost at an early design stage. However, due to the complex load cases closely dependent on the CFD, a complete and accurate 3D implementation of structural blade analyses has not been easy to achieve. The statement that 1D beam approximation will not be enough was already claimed back in 1990 in the review by Hodges [15], meaning that it should be even more accurate today when the computational capacities of computers have increased tremendously and more fidelity is desired.

On the other hand, new methods and approaches are still being developed. One promising approach was presented by Datta [22] and Staruk et al. [23] at the American Helicopter Society conference in San Francisco in January 2016. Preprocessing parts of this code were presented by Staruk et al. [17] at the American Helicopter Society forum in Montreal, Canada in 2014. The program called X3D was created in cooperation with the U.S. Army and University of Maryland and has found a first approach to couple a 3D finite element (FE) analysis and a thorough CFD analysis for an entire rotor hub, including joints, bearings, and composite blades. The hope is that this will lead to a better understanding of rotors and that it can be incorporated into the field of multicopter UAS where the blades have more complex geometries, varying chord and high camber. The modeling and analysis design can then be improved prior to building the vehicle, resulting in higher fidelity, increased safety, and better performance. The code is still under development, and the work and implementation of it into the field of multicopters will most likely continue in the near future.

4. Experimental Measurements of Quadcopter Rotor Blade Deflection

The experimental part of the project included two ways of measuring the out-of-plane deflection for a sweep of rotational speeds; the first method is the use of a Digital Single Lens Reflex (DSLR) camera and second one is by using tailored photogrammetry. The latter method had the advantage that it is possible to also measure the change in pitch of the blade. The method and setup of each approach is described in the following subsections after the theory section where the coning angle is derived. The coning angle gave an analytical value to the deflection that could be compared to the results from the experiments.

In this study two types of blades were examined, the plastic DJI Phantom 3 blade [24] and the carbon fiber reinforced T-motor 15x5 blade [4], both shown in Figure 2 below. The study focused on the plastic blades, while the carbon fiber ones were included for comparison of used models. The plastic blades are most likely injection molded thermoplastic blades with a diameter of 24 cm. The material properties were determined by tests, and the procedure and results are presented in section 5.1 Confirming Material Properties. The carbon fiber reinforced blades have a sandwich structure with a cork core, a plain fiber weave, and a diameter of 38 cm.

Figure 2: The two types of commercially available quadcopter blades that were studied. The top one is the carbon fiber T-motor 15x5 bade and the bottom one is the DJI Phantom 3 blade.

4.1 Theory: Blade Coning Angle

One of the more interesting components to look at in terms of blade deflection is the coning angle that occurs due to the rotation of the propeller. If there is a difference in pressure along the path of rotation, flapping occurs, meaning the blades deflect differently at different azimuths. For an isolated rotor in hover, which was tested here, this effect will not be present. The coning angle is the flapping angle in hover or the average flapping angle while in forward flight [25].

The forces acting on the blade cause them to deflect and assume the shape of a cone, as shown in Figure 3. Unfortunately, the only theory that exists for rotor blades is specific to full-scale helicopters, therefore the presented theory is derived for full-scale aircraft. Nevertheless, the theory can be used to understand the basic characteristics of blade deflection that are also present in small multicopter UAS, and to get a rough estimation of the deflection that can be used for comparison with experimental results.

The theory of rotating blade motion for helicopters, also known as Blade Element Momentum (BEM) theory, is well described by many authors, two of them being Leishman [25] and Johnson [26]. They both state that the three main forces acting on a rotating blade when it is spinning are centrifugal force, inertial force about a flap hinge, and aerodynamic force. Johnson [26] claims that the total moment acting on the blade during rotation will be:

$$\int_0^R m\,\Omega^2 \beta r^2 dr + \int_0^R m\ddot{\beta} r^2 dr + \int_0^R (dL) r dr = 0 \tag{1}$$

where m is the mass per unit length, r is in this case the normalized distance from the center of rotation, and β is the total flapping angle. For definitions, see Figure 3. The moment of inertia about the flap hinge is defined as:

$$I_b = \int_0^R r^2 m\, dr \tag{2}$$

This gives a simplification to Eq. (1) that can now be rewritten as:

$$I_b\left(\Omega^2 \beta + \ddot{\beta}\right) + \int_0^R (dL) r dr = 0 \tag{3}$$

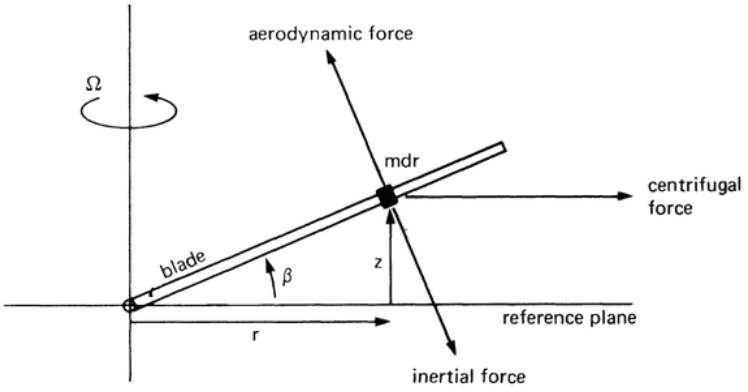

Figure 3: Definition of aerodynamic forces acting on a rotor blade and the change in blade flapping angle β [26].

This expression can be simplified further, and with the introduction of the Lock number, the coning angle, β_0, can be extracted. The Lock number is the dimensionless parameter that represents the ratio of aerodynamic forces to inertial forces and is defined as:

$$\gamma = \frac{\rho c C_{l\alpha} R^4}{I_b} \tag{4}$$

Even though the rotors of multicopters have rigid hubs, the spring hinge approximation for hingeless rotors can be used according to Johnson [26]. The rotor has a structural spring at the blade root, which approximately describes the rigid bending that occurs at the rigid rotor blade roots with a soft material. This means that Eq. (3) will need an extra spring stiffness term resulting in:

$$I_b\left(\Omega^2\beta + \ddot{\beta}\right) + K_\beta\left(\beta - \beta_p\right) + \int_0^R (dL) r dr = 0 \tag{5}$$

where β_p is the preconing angle and K_β is the spring stiffness, or more precisely the torsional stiffness of the material. The coning angle, β_0, for a rigid hub multicopter blade can then be derived from Eq. (5) and becomes according to Johnson [26]:

$$\beta_0 = \frac{\nu^2 - 1}{\nu^2}\beta_P + \frac{\gamma}{\nu^2}\left[\frac{\theta_{.8}}{8}(1+\mu) - \frac{\mu^2\theta_{tw}}{60} - \frac{\lambda_{NFP}}{6}\right] \tag{6}$$

Due to the hover mode and the geometry of the blades it can be said that $\mu = 0$ and assumed that $\beta_P = 0$. Hence the relation can be simplified to:

$$\beta_0 = \frac{\gamma}{\nu^2}\left[\frac{\theta_{.8}}{8} - \frac{\lambda_{NFP}}{6}\right] \tag{7}$$

where $\theta_{.8}$ is the pitch of the blade at 80 percent radius, ν is the dimensionless normalized natural frequency of the blades, and λ_{NFP} is the inflow ratio. The dimensionless natural frequency can be approximated [26] by:

$$\nu^2 = 1 + \frac{K_\beta}{I_b\Omega^2} = \frac{(I_b\Omega^2 + K_\beta)}{I_b\Omega^2} \tag{8}$$

While the inflow ratio at the no flapping plane can be approximated to the total inflow ratio, which for hover is simplified to:

$$\lambda_{NFP} = \lambda = \sqrt{\frac{C_T}{2}} \tag{9}$$

Here C_T is the thrust coefficient that can be approximated from performance measurements as:

$$C_T = \frac{T}{A\rho(\Omega R)^2} \tag{10}$$

Here T is the measured thrust, A is the area of the rotor disk, ρ is the density of the air, and ΩR is the rotor tip speed. This means that the relation for the coning angle in hover will depend on the rotational speed as follow:

$$\beta_0 = \propto \frac{A_1\Omega^2}{A_2\Omega^2 + A_3} \tag{11}$$

where A_1, A_2 and A_3 are constants.

Rotors that have hinges also experience lead-lag displacement, but due to the hingeless structure of the propellers used in multicopters, this phenomenon is not present and not studied herein.

4.2 Deflection Measurements Using DSLR Camera

The first round of measurements included simple out-of-plane deflection measurements along with various performance measurements such as RPM, forces, and moments on the smaller plastic rotors while in hover. A DSLR camera was used for capturing the images. The test was mainly focused on the plastic blade model as it was concluded that the deflections in the composite model might be too small to register with this technique due to the material stiffness. A single run was nonetheless completed for the carbon fiber blades to get a comparison to the unreinforced plastic blade.

The experimental setup consisted of a solid test stand, as shown in Figure 4 and Figure 5, on which a load cell was fastened. An isolated motor that is commonly used in multicopters was secured to the load cell, and finally the studied propeller was attached to the motor. All cables needed for the motor control, RPM readings, and load cell readings were connected and secured so that the airflow from the rotor would not be influenced too greatly by the cables. A camera was set up on a tripod and aligned to capture the profile of the rotation disk. Also, a lamp was added next to the camera for better light and contrast to facilitate the displacement extractions from the photographs.

The goal of the test was to measure the out-of-plane deflection for various RPM with an increase of 500 RPM for each point. This range was limited by the RPM reader for the lower values, and by the motor heating up for the higher values. Despite this, a good spread of data was obtained. The deflection study was made on five DJI Phantom 3 propellers, all counterclockwise rotors. The labels for the propellers were 1, 4, A, B, and C due to use of different batches. This way a small statistical sample could be established. For the carbon fiber T-motor blade only one run was performed on only one counterclockwise rotor. Specifications on range and camera settings are shown in Table 1.

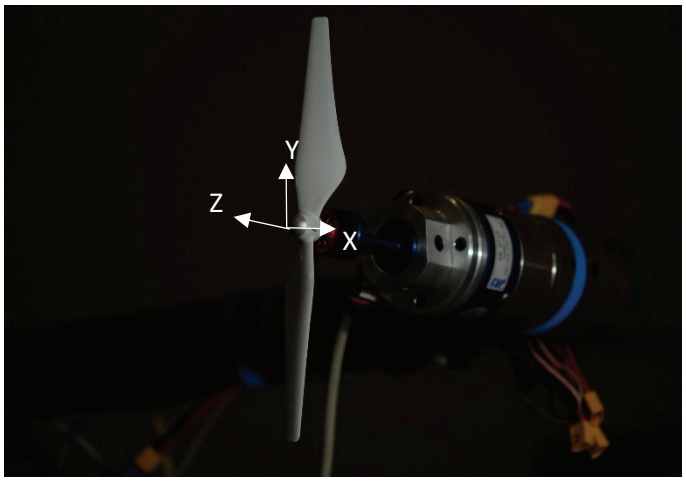

Figure 4: A close-up photo of the blade in the experimental setup for DSLR camera measurements for the DJI Phantom 3 propeller with the coordinates of the load cell.

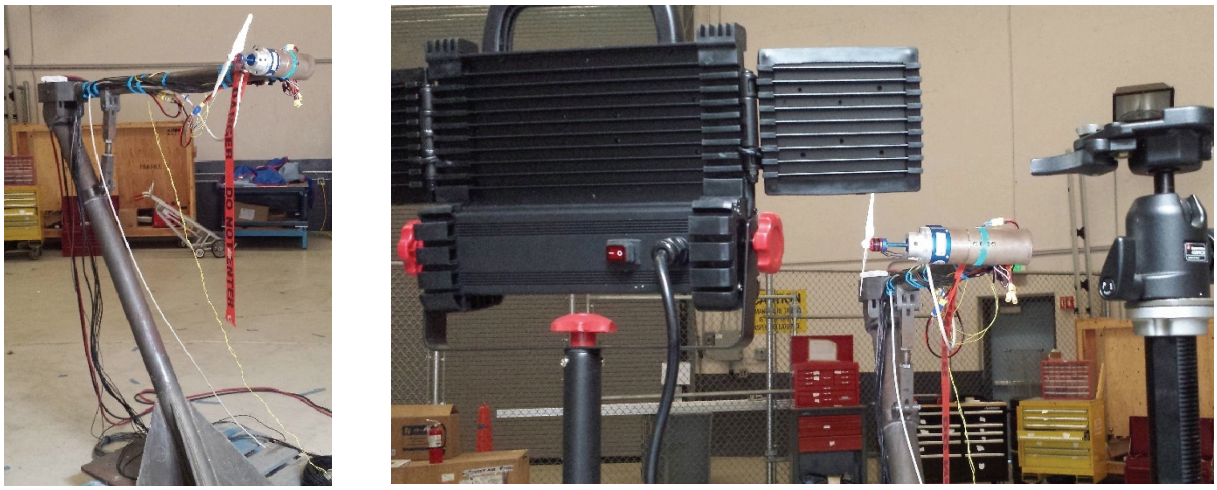

Figure 5: The test setup for the DSLR camera measurements with an isolated rotor fastened to the test stand.

Table 1: Specifications on the measurements for the DSLR camera test.

	DJI Phantom 3	T-motor
Number of Propellers	5	1
Propeller Labels	[1,4,A,B,C]	[1]
RPM Sweep Range	2500–8500	2000–000
Camera Exposure Time	1/90 s	1/90 s

The performance data was recorded with the NASA Basic Data Acquisition System (BDAS) with the help of a 6-degree-of-freedom load cell and voltage meters from which loads, moments, and RPM could be estimated. The rotational frequency was recorded, and a fast Fourier transform (FFT) was done within the software to receive the RPM. The deflection was, as mentioned earlier, recorded by photographing the profile of the rotating blades. With the help of a calibration board, a relationship between pixels and distance was established for future post-processing. This was done using the shareware application DataThief [27] where points of interest were approximated for each RPM. The points of interests were at the tip of the blades, as the deflection was greatest at these points. To prevent errors due to unplanned shifts in camera angles, a second stationary point was extracted to check that the camera still had the same position. If that was not the case, the difference was then used to compensate for that displacement. In the cases where the camera got shifted, a fixed point of the test stand was chosen on each photo so that the relative distances could be subtracted.

4.3 Deflection Measurements Using Photogrammetry

Photogrammetry is the art of determining the position of a target in a 3D space with the use of photographs and targets. The general idea is that by knowing the position of some stationary targets, the position of the targets of interest can be determined. The position of each target is determined by triangulation, meaning that by using more than one camera at different angles, a mathematical line can be drawn from each camera to the target. These lines cross, and the distance between the targets and the cameras can be calculated. Then the moving and displaced targets can be compared to stationary targets that build up a global reference system.

Targets that are used during photogrammetry are markings that are captured by the cameras and they can, for example, be simple retro-reflective material or laser grids. The retro-reflective targets need to be lit up on each photo take, which is usually done with the help of strobes. Targets can both be stationary or moving, where the former are known points to create a reference grid, and the latter could be on a point of interest whose exact location is not known in the measured space.

This method has been used for a long time and quite a few commercial systems are available, one being the automated system called VSTARS, while other systems are more custom built to fit the application. Photogrammetry is well suited for determining how loads will affect the deflection of a structure, as it has a higher fidelity than the DSLR method and better accuracy. The systems transform the results into a digital response that can be used for further post-processing.

4.3.1 VSTARS

The VSTARS system is a photogrammetry system made by Geodetic Systems, Inc. [28] that enables real-time measurements by using stationary targets and moving retro-reflective targets. The test targets on the moving blade had a diameter of approximately 3 mm, while the stationary targets were 6 mm in diameter.

The system uses calibration and coded targets to ensure a stable coordinate system, which enables the cameras to be moved around. The system that was used is called the VSTARS M system, which operates with two or more cameras and acts like a “portable optical coordinate measurement machine.” The cameras are high speed and the accuracy of the system is 1:60000 on a 4-m object [28]. Scale bars are used to get the proper scaling of the coordinate systems. Once the calibration is done, the software gives real-time positions of chosen targets from which the deflection and change in pitch can be determined. The setup is shown in Figure 6.

It was quickly determined that the VSTARS M system did not work for the test conditions needed for multicopter propeller analysis. In the system, each target is assigned a specific number and is tracked within a region of interest. For example, the VSTARS cannot, at this time, be set to use an external trigger to take a photo once every revolution, so it could not be determined what position the blade would be for each caption. This meant that the targets could not be tracked because the regions of interest of each target would be too big and would coincide with regions of interests of the other targets. It was concluded that this photogrammetry system is not yet applicable for the test setup used in this study. Instead a more tailored method was used as described in section 4.3.2 Tailored Photogrammetry.

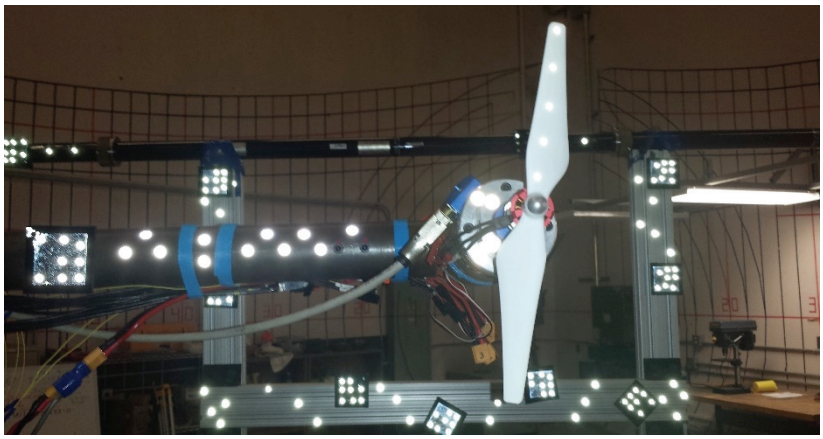

Figure 6: Illuminated targets on the blade and surrounding stationary points for the VSTARS photogrammetry test.

4.3.2 Tailored Photogrammetry

The tailored test was performed on a sweep of RPM with a step of 500, similar to the DSLR camera method. The specifications on range and number of photos is shown in Table 2. The range for the DJI Phantom 3 blades was modified, since a replacement motor was needed when the old one broke down during a test. To get statistical samples, several photos were taken for each RPM. Due to lack of time, only one carbon fiber blade was tested with only five photos per RPM.

During this photogrammetry test, two Imperx 4M15L cameras with a 135-mm lens were used with strobes that illuminated the targets. The system consisted of an external trigger that simultaneously triggered the cameras and then the strobes with a slight delay of 70 microseconds. The triggering pulse was set to a TTL pulse with a trigger duration of 0.2 ms. The pulse was released roughly once every second from a series of 1-per-revolution signals coming from the RPM meter. The image captured by the cameras was transmitted through an optic cable to a frame grabber and a computer. A dedicated software program was used to record the images of the two cameras. The images were then exported and post-processed with customized software used at NASA ARC, from which the coordinates of the targets in 3D space could be determined. From these coordinates the deflection and change in pitch angle could be determined. The hardware setup is shown in Figure 7.

Unlike the DSLR camera experiment, no performance measurements were taken, since the data acquisition system could not be incorporated into the external triggering of the cameras. The samples were taken for certain azimuths that depend on the magnetic poles of the motors and the RPM to ensure comparability between different speeds and blades. Due to an inconsistent RPM pulse coming in, the poles shifted slightly for the different RPMs. To get a proper comparison, a static photo was taken for each azimuth of interest to find the zero-lift reference. Calibration was implemented with a calibration plate where the in- and out-of-plane distances to the targets had been measured a priori. The camera details are shown in Table 3.

Table 2: Specifications on the measurements for the photogrammetry test.

	DJI Phantom 3	T-motor
Number of propellers	5	1
RPM sweep range	2500-7500	2000-5000
Number of photos	8	5

Table 3: Specifications on equipment used in the photogrammetry test.

Parameter	Value
Camera	Imperx 4M15L
Lens	135 mm
Trigger pulse duration	0.0002 s
Strobe delay	0.00007 s
Target size	1 mm

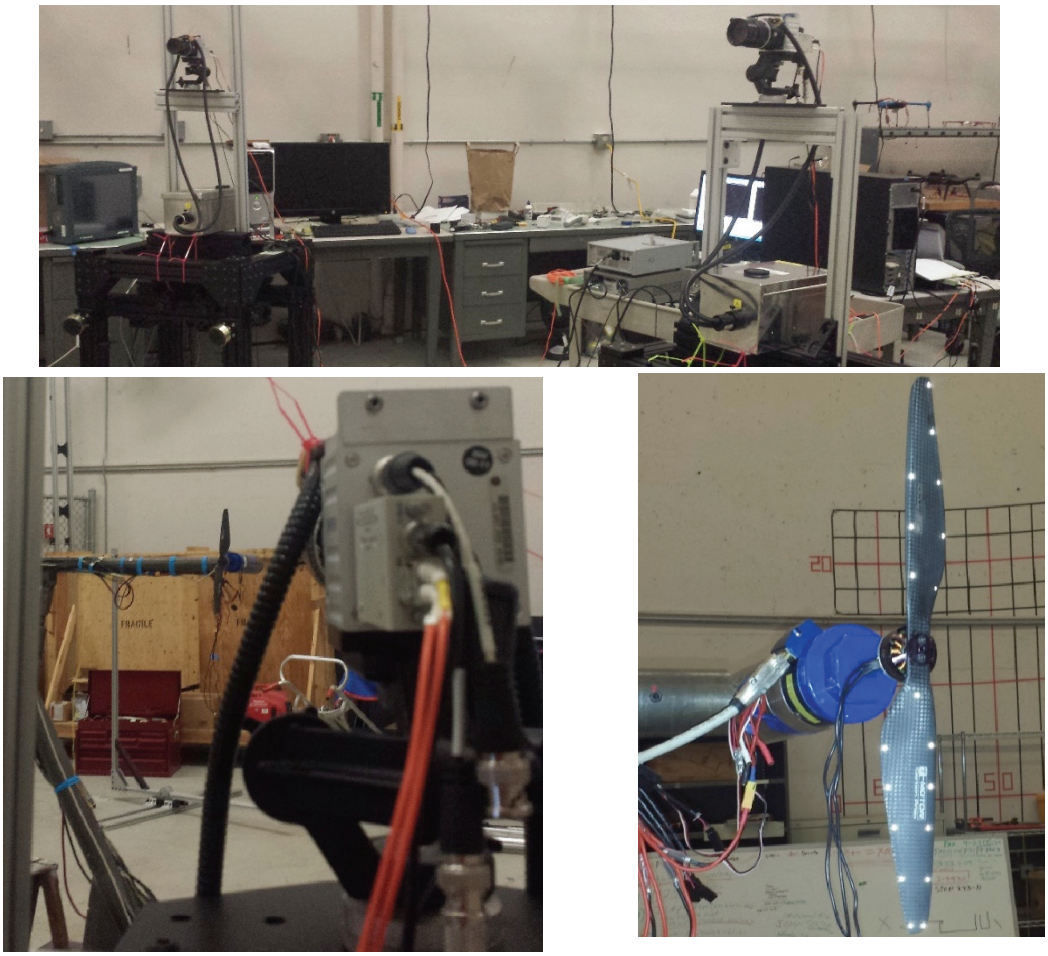

Figure 7: Tailored photogrammetry test setup. Top: Cameras with image acquisition and rotor speed control. Bottom left: View from camera to test stand. Bottom right: Isolated rotor on test stand with illuminated targets.

Circular targets with a diameter of 1 mm were used for the tests. This was considered small enough to not cause significant change to the structure and aerodynamics of the blade, and at the same time, big enough for the camera to capture and for the post-processing to recognize as targets. The target pattern was set so that two targets were placed at some radial stations, one on the leading edge and one on the trailing edge. To be able to distinguish the two blades on each propeller, one of them had an extra row of targets. This might have caused some balance distortion on the plastic blades, but it was considered small enough to not affect the results too severely. The target patterns for the plastic DJI Phantom 3 blades after the test were run are shown in Figure 8.

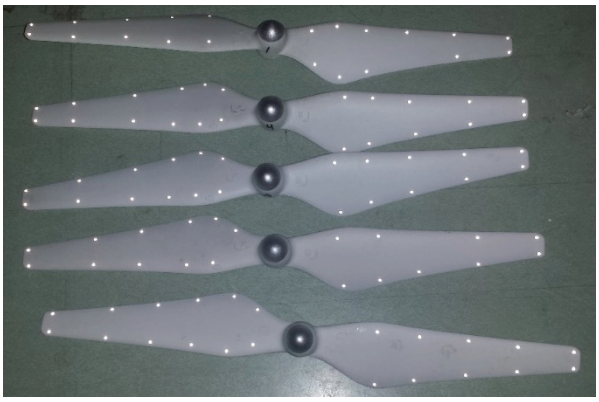

Figure 8: The five tested DJI Phantom 3 blades with illuminated targets. Some targets fell off during the higher RPM measurements.

5. Simulation of Blade Deflection Using FEA

The primary purpose of simulating the deflection is to see if software such as ANSYS, which is not designed for rotorcraft analysis, can be used to predict the coning behavior. If that is possible, then a 3D implementation in future codes should feasible. The simulation was done in two steps: first the material properties were confirmed, and second the actual isolated rotor hover was simulated. However, only one proper hover simulation model was considered.

5.1 Confirming Material Properties

Early on in the modeling phase, inconsistencies were found regarding the material of the DJI Phantom 3 blades. The manufacturer did not state specifics on which material was used other than that it was a "durable plastic" [24]. A bit of research among other producers of multicopter propellers showed that Nylon 6 and acrylonitrile butadiene styrene (ABS) were some of the commonly used materials. However, using the common material data of these materials resulted in a much lower mass of about 7 g compared to the 12 g of the actual product. Thus, there was a need to confirm the material's properties to be able to perform reliable hover simulation.

5.1.1 Static Bending Test

To validate the material, structural analysis was performed. This included a simple static structural bending case where the load was applied at the tip of the blade. The deflection was then compared to the one obtained in the lab where static loads were put on the blade. The blade was fastened on a motor that was secured to a solid plate. A static load was applied by fastening a string with weights on the blade. The defection was measured using the DSLR camera approach described earlier.

In the FE simulation, the load was applied to the face at the tip of the blade, while the boundary conditions included a homogeneous rotor made of one piece where the base of the hub had a fixed-support constraint. The mesh was an automated distribution of 7640 tetrahedral elements, where the maximum element size was set to 5 mm. The mesh convergence is shown in Appendix A—FEA Convergence Study, but resulted in a theoretical error of less than 1 percent. The resulting deflections for five different loads for the common Nylon 6 and ABS material properties are shown in Table 4, along with the results from the static bending test.

Table 4: Deflections for different loads for the two material types and from bending tests. ABS with ρ = 1080 kg/m^3, E = 2.25 GPa, and ν = 035. Nylon 6 with ρ = 1300 kg/m^3, E = 3 GPa, and ν = 0.4 [29].

Load [N]	ABS – Deflection [mm]	Nylon 6 – Deflection [mm]	Tested Material – Deflection [mm]	Bending Test – Deflection [mm]
0.18	6.1	6.0	1.4	1.7
0.36	12.2	11.9	2.9	3.1
0.54	18.3	17.9	4.3	4.3
0.72	24.4	23.8	5.8	5.7
0.90	30.5	29.8	7.2	7.1

Trial and error estimation was performed to find the elastic modulus that gave the best correlation between simulation and actual test. Since the material is a thermoplastic, the Poisson's ratio was set to 0.4, same as for Nylon 6 due to the resemblance of the materials. An elastic modulus of 9.5 GPa gave the best correlation, again shown in Table 4 under "Tested Material."

5.1.2 Material Determination of Plastic Propellers

The first step in determining material properties was to determine if any fibers were present in the material. This was done by cutting up test samples of the blades, polishing them, and looking at the surface through a microscope. Both the specimen close to the root and the specimen close to the tip showed the same structure, namely inclusions such as spherical granulates or maybe short fibers. This is clearly seen in Figure 9 and Figure 11. It was also concluded that the inclusions were most likely not voids, since a void would give a deeper hole and make it possible to see the material on the inside of it. A void can be seen as the darker spot in Figure 10 while the inclusions are magnified further in Figure 12, thus showing how more distinct the void is compared to the other dots.

It is believed that these inclusions are added to provide additional strength, which would be reasonable as thermoplastic materials have lower strength and elastic modulus. If they are spherical inclusions, then they could also be added to improve the flow characteristics of the resin. It could also be seen that the amount of inclusions is slightly higher closer to the wing tip (compare Figure 9 and Figure 11), at least in the studied photos. On the other hand, comparing these images with the injection molded Nylon 6 with short glass fibers that were studied in the paper by Bijsterbosch and Gaymans [30] could possibly hint that these inclusions are indeed short glass or polymer fibers. The spherical inclusions might have some minor effect on the material, but due to their size and roughly even distribution, it is assumed they gave the material isotropic properties and further information was not needed to perform FE simulations.

The second step included determining material properties by performing tensile tests. The goal was to find the E-modulus of the material under the assumption that the material is isotropic. The tensile test was made with only 2 test specimens, mainly due to lack of time and that the first specimen had traces of sliding during the test. The strain was measured using Digital Speckle Photography (DSP). A specimen with a length of about 10 cm was cut out from the propeller in a section with the most even thickness. Glass fiber and vinyl ester composite tabs were glued with Araldite 420 adhesive to the specimen to avoid twisting and shearing.

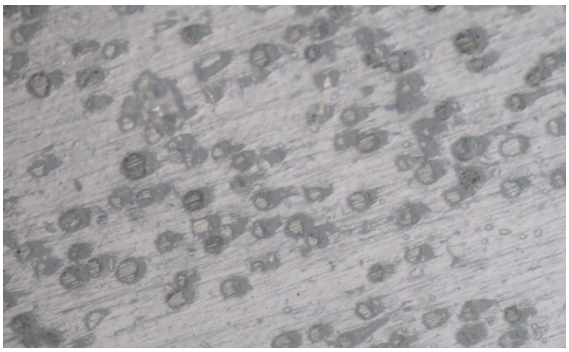

Figure 9: 5x magnification of specimen from blade tip with clear circular dots that were determined to be spherical reinforcement particles.

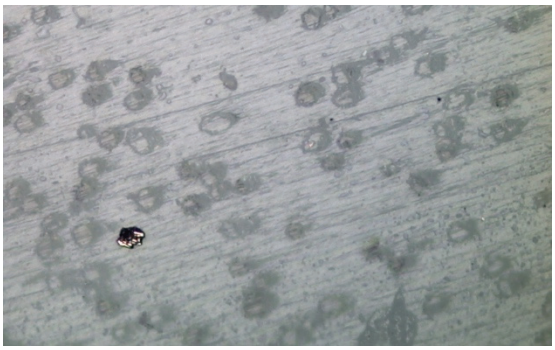

Figure 10: 5x magnification of specimen from blade tip with a void present (dark circle).

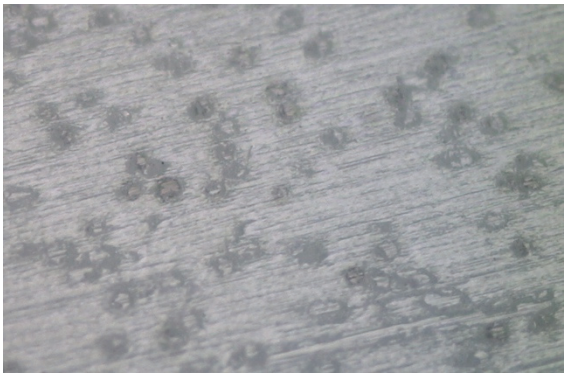

Figure 11: 5x magnification of specimen from blade root.

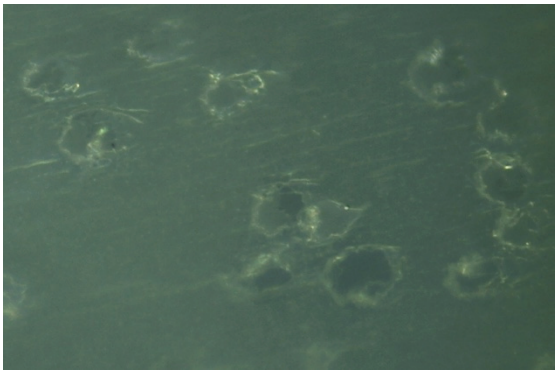

Figure 12: 20x magnification of specimen from blade root.

The specimen was mounted into a tensile testing machine (Instron 4505 with Instron 5-kN load cell) and was put to a deformation of 0.1 mm/s. An Aramis DSP system was then used for 2D measurements of the resulting position movement and post-processed to give the strain. From that, the cross-section area was determined from the CAD model and the elastic modulus was approximated to 6.5 GPa. Here the material was assumed to be isotropic (due to randomness in inclusions) and linear elastic. It was also assumed that the material kept its initial cross-section area and that the stresses in the material were isotropic. The elastic modulus was then approximated from the initial linear part of the load-position curve due to the less than ideal loads that the propeller is exposed to during usage. See Figure 13 for test setup, specimen, and resulting load-position curve.

To conclude, it was not possible to determine the exact material of the blades without more in-depth tests, but it can be said that it was a thermoplastic (much likely ABS or Nylon 6) with spherical inclusions. The Poison's ratio was again approximated to 0.4. The material properties were measured to be E = 6.5 GPa, which can be seen as a lower material limit due to difficulties in the measurements. This could be compared to the Young's modulus of 2–3 GPa for pure Nylon 6 and the 14 GPa of 30 percent glass fiber reinforced Nylon 6 [31].

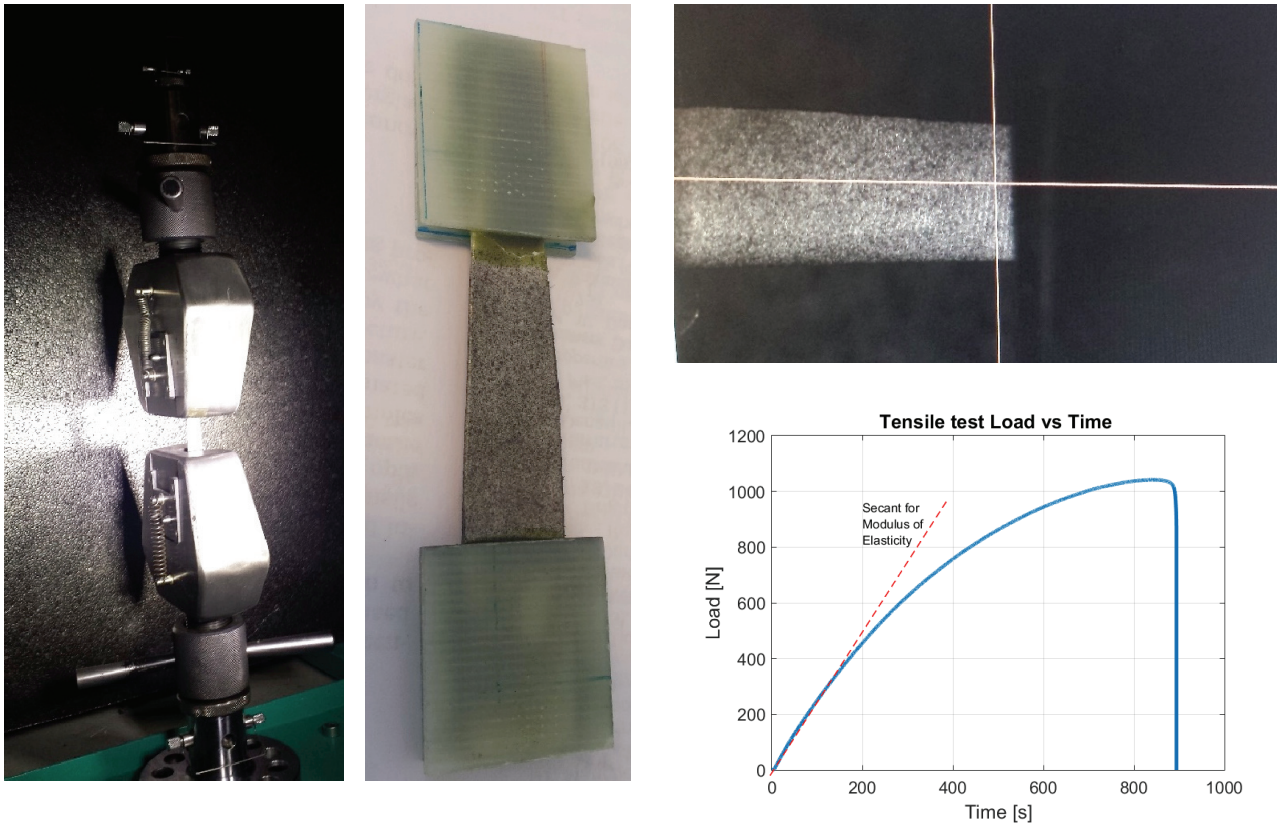

Figure 13: Left: Setup for tensile test with Instron machine. Middle: Test specimen with speckles for DSP measurements and tabs. Right upper: Close-up photo of the resulting DSP image. Right lower: Resulting load-time curve for test specimen 2.

5.2 Simulation of Blade Deflection

This study was made to investigate the possibility of simulating the deflection of rotor blades using 3D FEA in ANSYS Workbench. The only two forces that could be applied as default in ANSYS were the effects of inertial and centrifugal force. Unfortunately, due to lack of time and knowledge, no CFD was performed to get the exact aerodynamic loads. The lift force was instead modeled through the theoretical lift distribution, described in section 5.2.1 Theory: Lift Distribution. The two blade types were only studied at one RPM each, 7500 for the DJI Phantom 3 and 5000 for the T-motor.

5.2.1 Theory: Lift Distribution

The loads that act on a multicopter are, as mentioned, the classical aerodynamic loads such as thrust, drag, weight, and lift. Due to the rotating blades, some parts of the drone will also experience torque. The blades, however, will mainly experience lift and drag along with inertia due to its mass and finally centrifugal force due to the rotation. The theory of rotorcraft aeromechanics is thoroughly described by Leishman in reference [25], and the equations presented in this section follow that format unless stated otherwise. The spanwise lift distribution, dL, on the blade, where the span is along the y-axis, can be described by:

$$dL = \frac{1}{2}\rho U_y^2 c_y C_{l_y} dy \tag{12}$$

Here ρ is the air density, c_y is the local chord, C_{l_y} is the local section lift coefficient, and U_y is the local section velocity of the air passing the blade. Since the out-of-plane velocity is much lower than the tangential velocity, the following approximation can be made for the spanwise distributed section velocity U_y:

$$U_y = \sqrt{{U_y}_T^2 + {U_y}_P^2} \approx {U_y}_T = \Omega y \tag{13}$$

where y is the radial distance from the hub center of rotation and Ω is the angular frequency of the rotor.

Furthermore, the spanwise lift coefficient for a distance y from the center of rotation can be approximated as:

$$C_{l_y} = C_{l_\alpha}(\theta - \alpha_0 - \phi) = C_{l_\alpha}(\theta - \alpha_0 - \frac{\lambda_y R}{y}) \tag{14}$$

since small angle approximations are made and the total inflow angle is:

$$\phi_{total} \approx \frac{U_P}{U_T} = \lambda \tag{15}$$

Here $C_{l_\alpha} = 2\pi$ is the slope of the lift vs. angle-of-attack curve, θ is the pitch angle, α_0 is the corresponding zero lift angle, ϕ is the relative inflow angle, λ_y is the inflow ratio at certain radius, and R is the total radius of the rotor. The definitions of the inflow ratio were described in section 4.1 Theory: Blade Coning Angle, and the definition of the angles are shown in Figure 14.

In the case of highly cambered and twisted blades, such as those of multicopters, these angles might vary along the span, as does the inflow ratio.

The spanwise inflow ratio will therefore be:

$$\lambda_y = \frac{\sigma C_{l_\alpha}}{16}\left[\sqrt{1 + \frac{32\theta y}{\sigma C_{l_\alpha} R}} - 1\right] \tag{16}$$

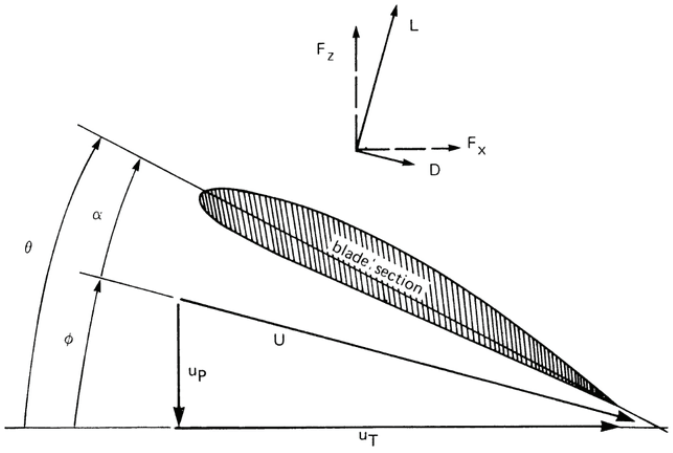

Figure 14: Blade cross section with defined angles and velocity components as well as lift and drag definitions [26].

Here σ is the solidity of the rotor defined as the ratio between the total blade area of N_b number of blades, assumed to be more or less rectangular with chord c, and the rotor disk area:

$$\sigma = \frac{N_b c R}{\pi R^2} = \frac{N_b c}{\pi R} \tag{17}$$

In a similar manner to lift, the spanwise drag distribution can be described as:

$$dD = \frac{1}{2}\rho U^2 c_y \, C_{d_y} dy \tag{18}$$

where C_d is the drag coefficient. However, since the drag is at least one order of magnitude lower than the lift, as presented by Leishman [25], it was neglected in this analysis. This means that in hover, the lift equals the produced thrust.

5.2.2 FEA Model

The geometry of the plastic DJI Phantom 3 blade was obtained from a 3D scan that was converted into a geometry file. The model is shown in Figure 15. This way the outer bounds of the geometry could stay more true to the original state than if the model was created by approximating an airfoil section and drawing it in a CAD program.

The carbon fiber T-motor blade was modeled in PTC Creo Parametric because no 3D scan of the blade was available. Measurements were taken for nine cross sections, and the airfoils corresponding to those sections were approximated. This means that the actual outer geometry could only be as good as the approximations, which had some flaws in determining pitch angle and exact airfoil geometry.

The material used in the simulations is shown in Table 5. The properties of the DJI propellers are from the tensile tests and FE static bending test described previously, while the properties of the T-motor propellers are estimated according to what the manufacturing stated as the material and the common values corresponding to their material data. The fiber composite skin in the T-motor propellers was modeled as a transverse orthotropic material, but the true fabric weave was not possible to recreate.

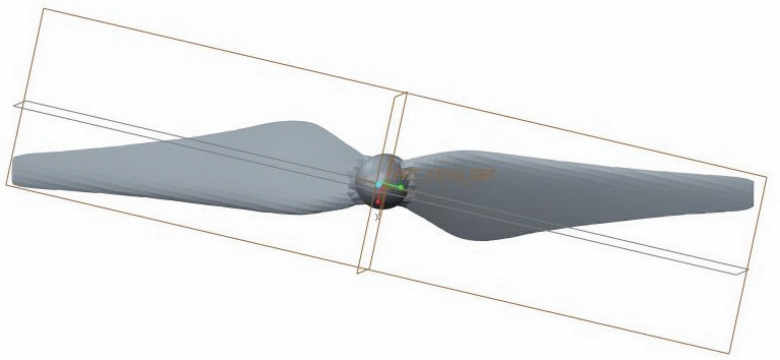

Figure 15: The CAD model resulting from a 3D scan of the 24-cm plastic blade.

Table 5: Material properties of the studied blades.

Property	Material 1 – DJI Blades		Material 2 – Carbon Fiber Epoxy Woven Mat		Material 3 – Cork
$\rho\ \left[\frac{kg}{m^3}\right]$	1600		1550		150
$E\ [MPa]$	6500	9500	E_1	62700	20
			E_2	62100	
			E_3	8000	
G [MPa]	–	–	G_{12}	5000	10
			G_{13}	2700	
			G_{23}	2700	
ν	0.4		ν_{12}	0.1	–
			ν_{13}	0.1	

* For the DJI propellers, the two elastic modulus represent the one from the tensile test and the one from the static bending simulation. The fiber composite was estimated to be a T-300 3k/934 plain weave fabric with 60 percent fiber fraction since it is a material commonly used in aerospace applications and a reasonable approximation to the carbon fiber/epoxy weave fabric that the manufacturer states as material [4]. Material properties for carbon fiber and cork are from references [32], [33], and [34].

The mesh for the DJI model consisted of 8129 elements and the element type was set to Solid187, meaning a 10-node tetrahedral element. The elements were set to have a maximum size of 4.5 mm, but otherwise the automated mesh was used due to a non-sweepable geometry. A mesh convergence study was performed and resulted in a theoretical error of approximately 1.2 percent, which was considered acceptable. The approach and numerical results are shown in Appendix A—FEA Convergence Study.

As mentioned earlier there were three main loads applied to the model; lift, inertial, and gravitational. The lift was approximated with the theoretical model, Eq. (12) described in the theory section, and modeled as a surface loads that were applied to the lower faces of the blades. The distribution was divided into 21 regions per blade for the plastic DJI Phantom 3 blade, as it seemed to fit the model fairly well. The inertial forces were applied through a rotational velocity with a certain RPM and a standard gravity. The boundary conditions included a simple support in the vertical and radial direction, while it was free to move in the rotating direction. The constraint was located at the bottom and on the inner sides of the hub, where the propellers are attached to the motor, thus describing the real rotation rather well. The summary of the two blade models is shown in Table 6.

Table 6: Details about FE models for the two blade types.

	DJI Phantom 3	T-motor
RPM	7500	5000
Total Lift [N]	2.9	9.9
Sections	21	8
Elements	8129	22284

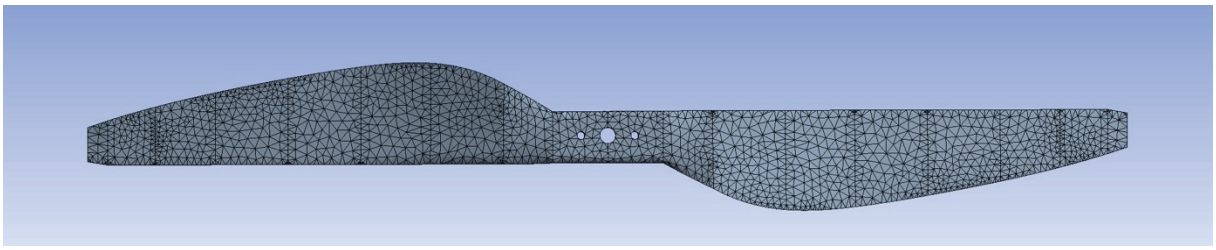

Figure 16: The meshed CAD model of the T-motor blade showing the 8 regions on the blade where the forces were applied.

A similar setup was made for the carbon fiber blade with a corresponding lift distribution, this time for eight regions per blade. The number of elements was 22,284, and element type was again set to Solid187. Contact elements were also added due to the use of core and orthotropic materials. The elements were also oriented so that they would represent the weave of the fibers. The mesh convergence study showed an error of 1.8 percent, and the resulting mesh is shown in Figure 16. For more detail, see Appendix A—FEA Convergence Study. In this model, a similar simple support was added at the main hole where the blade is attached to the motor as well as an extra out-of-plane displacement constraint at the two smaller holes where additional screws attach the blade to the motor.

6. Results

The results obtained by the two experimental methods are presented below, followed by an analytical solution for the coning angle for comparison. After that, the results from the FEA simulations are presented. When more than one propeller was tested, or more than one test was performed, the arithmetic mean value was calculated as:

$$\mu = \sum \frac{x_i}{M} \tag{19}$$

along with the standard error of the mean:

$$s_\mu = \frac{\sqrt{\left(\frac{1}{N-1}\sum(x_i-\mu)\right)^2}}{\sqrt{N}} \tag{20}$$

where x_i is each measured value and N is the total number of samples.

6.1 DSLR Camera

The results from the DJI Phantom 3 blades point towards a linear or possibly negative quadratic relation for the studied sweep range that did not include the zero deflection at 0 RPM. This can be seen both in the sample of five counterclockwise blades, Figure 17, and the study of the first blade only, Figure 18. The maximum deflection tends to be up to a mean value of 4 mm for the highest RPM of 8500 with up to 0.16 mm standard error of the mean, in accordance to Eqs. (19) and (20). For 7500 RPM, the deflection has a mean value of 3.7 mm and a standard error of the mean of 0.16 mm. The exact numerical results are shown in Appendix B—Numerical Results, DSLR Camera Measurements. The performance results, meaning the lift force during the measurements, are shown in Appendix D—Performance Results.

The coning angle of the blades clearly follows the displacement curve for different RPMs due to the simple trigonometric relation between these and the small angle approximations. The coning angle reaches up to about 2 degrees, which is shown in Figure 19 and Figure 20.

For the carbon fiber T-motor blade, only one run was made to get a comparison to the FEA results. The results tend to show a maximum deflection of 2.2 mm with a coning angle of 1.1 degrees at 5000 RPM, which is shown in Figure 21.

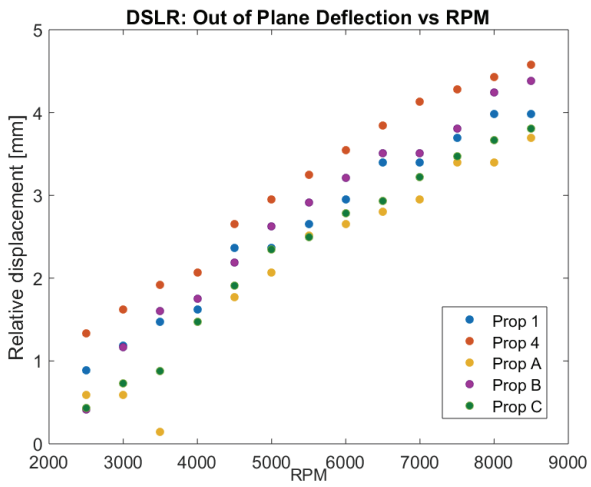

Figure 17: Relative displacement for the five DJI Phantom 3 blades acquired with DSLR camera measurements.

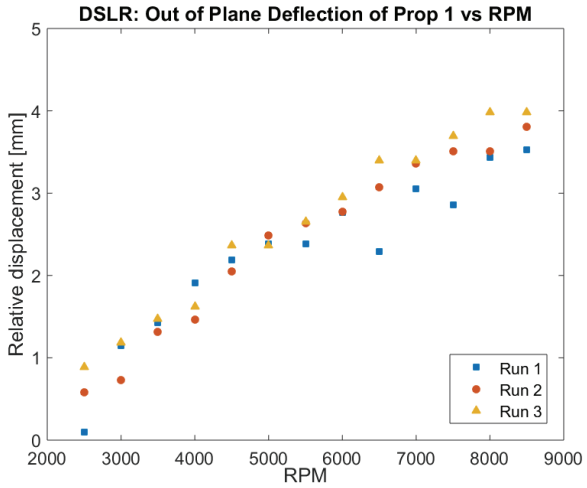

Figure 18: Relative displacement for DJI Phantom 3 propeller 1 acquired during three runs with DSLR camera measurements.

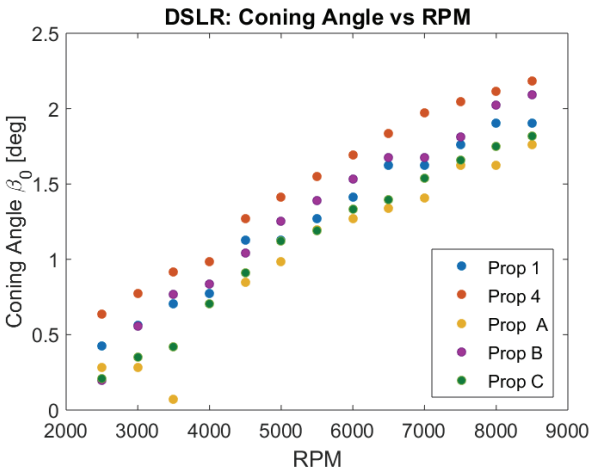

Figure 19: Corresponding coning angle for the five DJI Phantom 3 blades acquired with DSLR camera measurements.

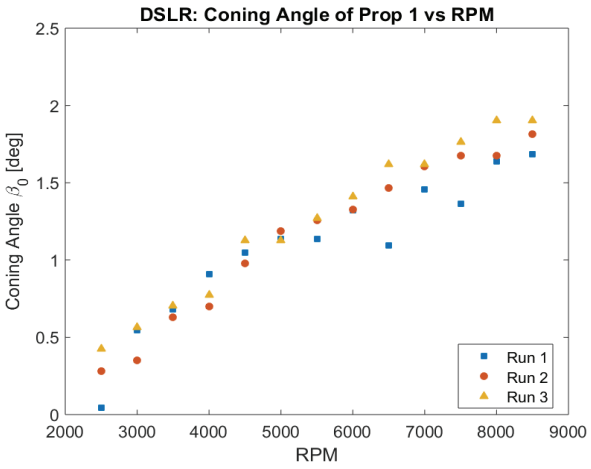

Figure 20: Corresponding coning angle for DJI Phantom 3 propeller 1 acquired during three runs with DSLR camera measurements.

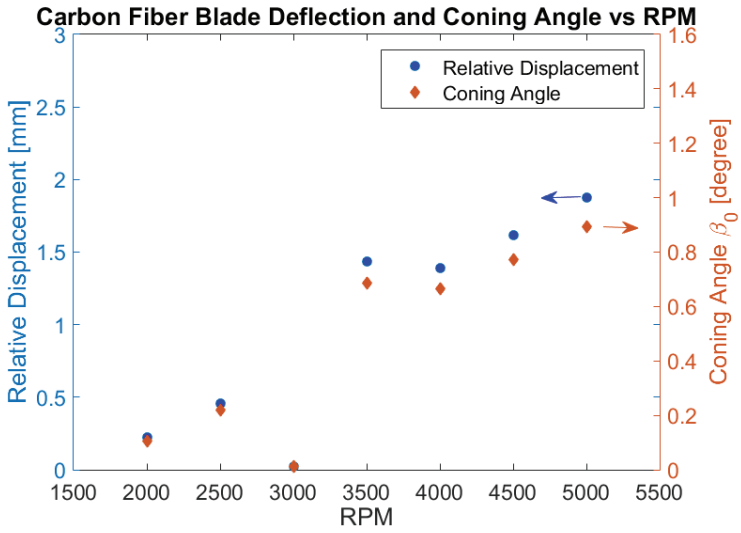

Figure 21: The relative displacement and coning angle for the T-motor propeller from DSLR camera measurements.

6.2 Photogrammetry

The following results are from the tailored photogrammetry described earlier in section 4.3.2 Tailored Photogrammetry. A mean value and a standard error of the mean were determined for each propeller at each RPM. For the plastic DJI Phantom 3 blades, the relative displacement at the leading edge of the tip was once again found to be between 3.5–4 mm, with a standard error of the mean of roughly 0.02 mm for most propellers at 7500 RPM. The corresponding coning angle is then 1.8–2.1 degrees. Both are depicted in Figure 22 and Figure 23. The individual mean results for each blade at each RPM are shown in Appendix C—Numerical Results, Photogrammetry.

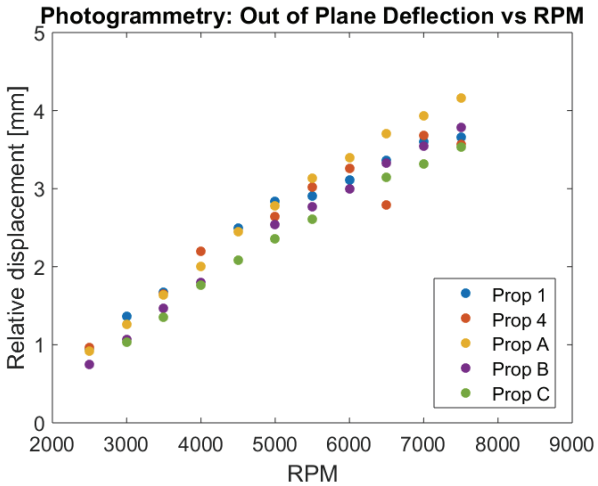

Figure 22: Relative displacement for studied RPM for the five DJI Phantom 3 propellers acquired with photogrammetry.

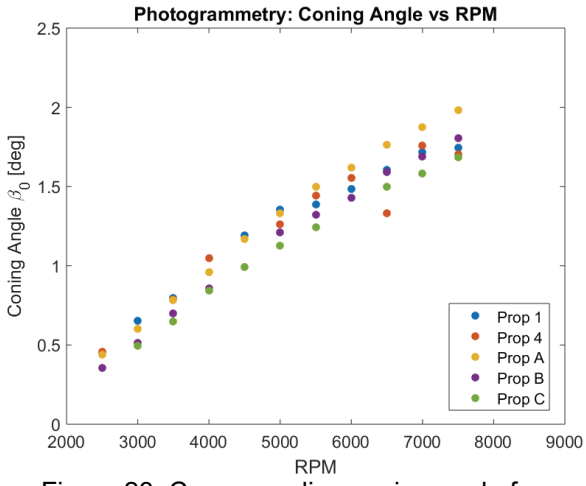

Figure 23: Corresponding coning angle for studied RPM for the five DJI Phantom 3 propellers acquired with photogrammetry.

For certain RPMs, the results had to be excluded as it was determined during post-processing that the some positions did not work well with the calibration. This became clear when some of the resulting positions calculated with the dedicated software were unreasonably large, as much as a factor 10 larger than the other positions. This was unfortunately discovered after the test was completed and no more runs could be performed. The excluded measurements for both the deflection and the change in pitch angle were: 4000 RPM for propeller 1, 4500 RPM for propeller B, and finally 2500 RPM and 6000 RPM for propeller C. At some RPMs there were still more than three approved runs, so these were included; however, they have slightly lower fidelity due to the smaller sample.

The change in pitch was calculated at the second pair of targets from the tip, about 15 mm, due to problems with many of the trailing edge targets. The results from the DJI Phantom 3 blades are shown in Figure 24, where a trend of decreasing pitch can be noted but scatter is present. A negative angle means that the leading edge has a lower out-of-plane deflection than the trailing edge.

For the carbon fiber T-motor blades, it was found that the deflection reached up to a mean value of 1.3 mm and a coning angle of 0.4 degrees for the highest measured RPM of 5500, as shown in Figure 25. The results for 2000 and 2500 RPM showed such low displacement that it was basically zero. For the 3500- and the 4500-RPM cases the values do not follow the assumed linear to quadratic shape from the DSLR measurements. For the stiffer T-motor blades, the pitch angle does not have a noticeable change but there are some large numerical errors for the lowest RPM (Figure 26). Again, the individual mean results at each RPM and the standard deviation are shown in Appendix C—Numerical Results, Photogrammetry.

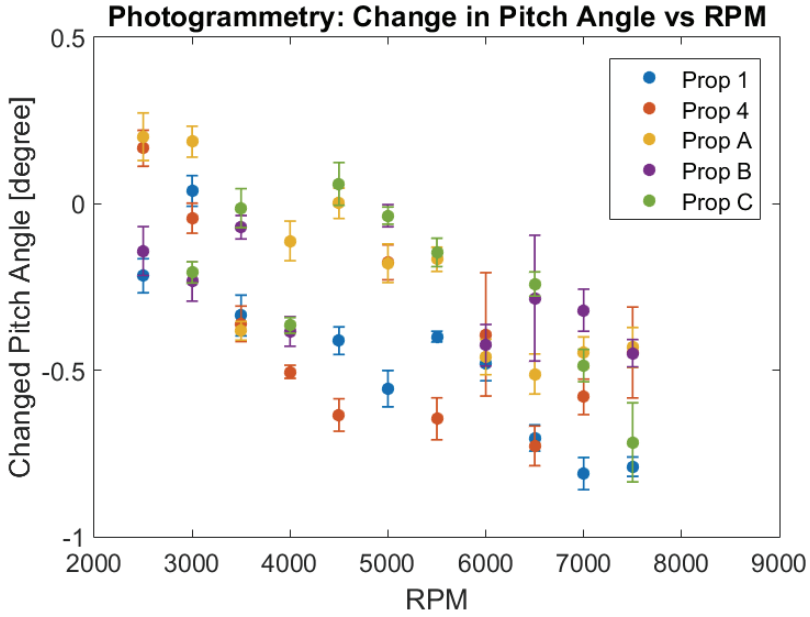

Figure 24: The change in pitch angle between leading and trailing edge for DJI Phantom 3 propellers.

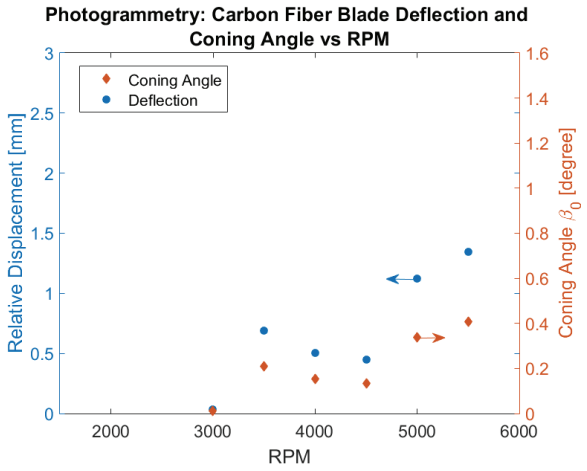

Figure 25: The deflection and coning angle for the T-motor blade.

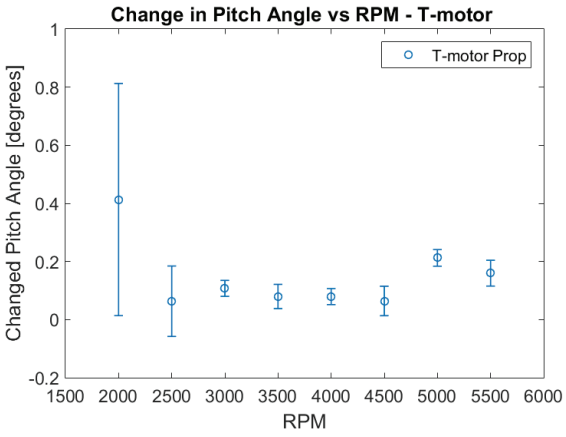

Figure 26: The change in pitch angle between leading and trailing edge for the T-motor blade.

6.3 Analytical Solution

The Blade Element Momentum (BEM) theory, especially Eqs. (5) and (7) presented in section 4.1 Theory: Blade Coning Angle, was used to find the analytical solution to the blade deflection coning angle. The theoretical relation between coning angle, and thus displacement, highly depends on the properties of the blade such as the torsional spring stiffness and the mass moment of inertia. If the inertia is very low, the relation becomes more quadratic, while if it is just slightly higher, it shifts over to linear or negative quadratic. For the spring stiffness, the case is the opposite.

Since some of the parameters could not be estimated, simple tests and FEA analyses were used to determine some parameters such as the natural frequency and the torsional bending stiffness. The angle of attack at zero lift was approximated using the airfoil analysis tool XFOIL [35] on the airfoil section at the determined radial stations. The results of the characteristics, i.e. Eq. (11) with constant A1 set to 1, are shown in Figure 27 where a clear negative quadratic relation is present for both blades. In Figure 28 the theoretical coning angle containing all the different constants is presented. The values of the constants and parameters, which were found by approximations and FEA simulations, are shown in Table 7.

Table 7: Parameter values used for the analytical solutions.

Parameter	DJI Phantom 3	T-motor
I_b	$7.66*10^{-6}$	$1.10*10^{-4}$
K_β	1.8	9.7
λ_{NFP}	0.08	0.07
$\theta_{.8}$	8°	6.5°
γ	3.92	2.29
Number of sections	7	8

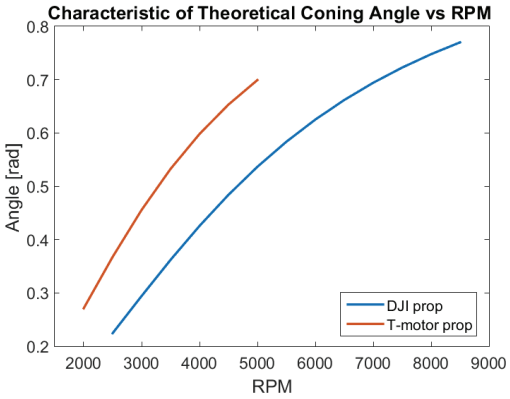

Figure 27: General characteristics of coning angle and RPM dependence with constant A1 = 1 for the two blade types.

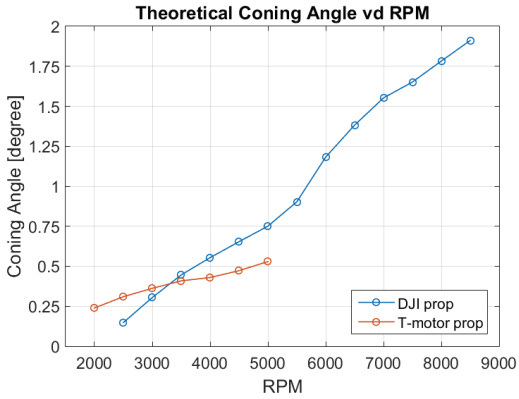

Figure 28: Theoretical coning angle vs. RPM with all constants.

The torsional stiffness could be determined from the simple FEA bending test that was also used to confirm material properties. To compensate for the cambered airfoils, the angle of attack at zero lift was subtracted from the pitch at 80 percent radius, similar to the way the lift distribution was compensated in Eq. (14).

6.4 FE Hover Simulation

In this section, the results of the hover simulations are presented for the two blade types subjected to loading in accordance to section 5.2.2 FEA Model. For the DJI Phantom 3 propeller, the resulting out-of-plane deformation was 3.6 mm for the estimated own material and 5.2 mm for the material from the material test. For the T-motor 15x5 propeller, the deflection was almost 2.6 mm, which is higher than both the photogrammetry and the DSLR results. These results, with the corresponding change in pitch angle, are shown in Table 8. The pitch angle was approximated at the studied RPM from the leading and trailing edge coordinates and deflections, where a negative angle means that the leading edge has a lower out-of-plane deflection than the trailing edge.

Table 8: Results from hover simulations for the two models.

Model	RPM	Out-of-Plane Deflection [mm]	Change in Pitch [deg]
DJI Phantom 3 – Experimental Material	7500	5.20	0.23
DJI Phantom 3 – Own Material	7500	3.62	0.16
T-motor	5500	2.57	0.31

7. Discussion

This section discusses and analyzes the results and the entire project. It starts with a comparison of the different measurement results and their comparison to the theoretical models. After this, the validity of the applied theory is discussed, followed by an evaluation of the measurement methods and an evaluation of the simulation model. To conclude, there is a discussion of recommended future work, and the importance of the results and how they can be used in multicopter product development.

To begin with, the different methods used to measure the out-of-plane deflection for the two types of blades provide a good opportunity to compare and evaluate said methods. When looking at the out-of-plane deflection of the DJI Phantom 3 blades, the results of the tailored photogrammetry approach show that the general characteristic of the relation between the deflection and RPM is found both by the theoretical approach and the DSLR camera test. In addition, the deflection is within the same range for all methods, but the spread in data between the five propellers is much smaller for the photogrammetry. Hence, it can be concluded that the linear-to-negative quadratic relation of deflection vs. RPM for the studied range is reasonable.

For the carbon fiber T-motor blade, the results between the two methods do not correspond as well. First of all, the results have some scatters. Secondly, the results for the lowest RPM were so small that it could not be guaranteed that the errors exceed the true values. However, the photogrammetry results for the higher RPM are considered more reliable due to the lower fidelity of the DSLR method for the T-motor blades. This would also be more reasonable, since the T-motor blades are much stiffer and should have a much smaller coning angle, where for the DSLR results the coning angle is almost a factor 2 higher. The correspondence with the theoretical results for the photogrammetry results are better, but due to lack of exact material properties and a high-fidelity 3D scanned CAD model, the constants had more approximations than the DJI propellers. Two such approximations are the pitch angle and angle of attack at zero lift that were calculated from the CAD model, which in turn was modeled using approximations of airfoils and angles. This all adds up to errors that slightly over predict the theoretical values. The relation between the RPM and the out-of-plane deflection was nevertheless found to be more linear to positive quadratic.

How these results would look in the lower ranges from zero to the staring sweep range of 2500 and 2000 RPM, respectively, should also be discussed. It is clear that at 0 RPM there is no deflection, but the devolvement of it up to these values could point towards a more quadratic relation so that it then transfers to the more linear relation found in the measurements.

When analyzing the individual results of the different methods, some anomalies could be seen in the DSLR measurements. The most noticeable is that the blade straightened out for DJI propeller 4 for RPM 3000 and 3500. A reason for this is not clear, but it is suspected that the blade was not perfectly balanced and was wobbling on the motor, which resulted in a lower deflection value. The support for this theory is that blurry double shadows were seen in the photos. The performance data from the DSLR measurements show higher power usage for higher RPM for the plastic DJI blades 4, A, and B. This means there should be a higher deflection at those values, which is also seen in the results for propeller 4 and B. However, for propeller A the case is slightly different, as all the values are shifted to higher deflection. It is suspected that the reason might be unbalance in this propeller, together with how the points were extracted. On the other hand, the photogrammetry results show higher values for propellers 4 and A, meaning that the measurements could be more sensitive than expected to surrounding conditions such as temperature and air pressure. Another cause of the slight differences might be that the added targets and their relative positions could have some effect on the stiffness and aerodynamic properties of the blades. The results

could also mean that the blades have such low quality that it will affect each run and position at which the measurement is taken. Blade quality is discussed further, later in this chapter.

The photogrammetry results unfortunately have some anomalies as well. As mentioned in section 6. Results, some measurements had to be excluded due to values being a factor 10 or higher—too high for some targets in some photos. It is suspected that photos at some angles, in combination with the used calibration and automated target numbering in the software, resulted in these inconsistencies. Another aspect could be the field of view of the cameras with the current setup that might have been at too small of an angle towards the target at certain azimuths. Adjusting the camera positions might have improved the results.

Continuing with the pitch angle results, the results have a more noticeable spread for all the DJI Phantom 3 blades. Even though there is a trend that the pitch angle between the leading and trailing edge decreases, the results of each blade have scatters of low and high values for the studied RPM. It is once again believed that this is partly to do with the calibration, azimuth angles at which the photos were taken, and the target numbering problem. Another aspect here is that two targets were used for calculating the angle, meaning that the errors in both targets will combine to an even bigger error. Also, even though the standard error of the mean is low, it does not necessarily mean that when combining the two targets, with rather small errors themselves, the resulting error will be small.

For the T-motor blades, there is not much change in pitch, which is reasonable due to them being stiffer. However, the results do show a small increase in pitch. This might be a measurement error, just as in the case of the DJI Phantom 3 propellers, but it could also be the way the blades behave. The first two values have a very large standard error of the mean, but that is suspected to be partly the result of the very small changes in displacements for these lower RPMs that give an error due to the small angle changes. Therefore it is recommended to first improve and reduce the measurement errors before any proper conclusions regarding the relation between change in pitch and RPM can be made for these types of propellers.

It should be mentioned that the measured angles are very small due to the small distance between the leading and trailing edge in the plane, but more importantly because of the even smaller out-of-plane distance. This means that even though the in-plane distance was assumed to be unchanged, the smallest error in out-of-plane distance will affect the calculated change in pitch. If there is then even some small imbalance in the propellers, due to for example blade quality or small changes in air flow due to the experimental setup, the photos at different azimuths might have small differences in target out-of-plane location that give rise to errors when calculating the change in pitch.

Much can be drawn from the methods of measurements of the studied blades themselves. The studied rotor blades had their difficulties when it comes to geometry and quality. The plastic DJI blades had the main problem of inconsistent quality, which was clearly seen in the results where five different blades were investigated and the difference in deflection could be up to 1 mm for the highest RPM. It is not entirely surprising that these cheap, mass produced blades might have differences in the mass distribution, balance, and even outer geometry. This is clearly shown in Figure 18 where the same blade was tested three times, with only somewhat different light settings, and showed a spread of almost 0.5 mm in the results. For the composite T-motor blade, the quality is assumed to be better, due to better material and higher price, but unfortunately that could not be confirmed as only one blade was tested.

Starting with the DSLR method, it can be said that the method has rather low fidelity. There are many sources of error, such as data point extraction and sharpness of the photos, and the numerical errors from the data extraction program (about 0.13 mm with current calibration) were relatively high. The determination of a suitable experimental method was an iterative process, since finding good test conditions together with good photo quality for easier extraction was not obvious at the start. Even though a satisfactory method with acceptable photos was achieved in the end, the method of choosing a data point was not obvious due to a boundary of pixels between different objects. Eventually, it was concluded that dark surroundings and one single bright light would work best for the plastic blade and a slightly lighter surrounding worked for the carbon fiber blade. This resulted in much better photos for the first case. For the second case, it was still nearly impossible to see the contours of the blades at higher RPM, meaning that the extraction of data points had a lower fidelity and could have resulted in the higher values. It was also noted, in some of the photos, that a second shadow was present. This could mean that the blades were not balanced, thus making some of the point extraction rather complicated. The situation was slightly better with the carbon fiber blades, as their quality is overall better, yet at the same time the twist at the top made pinpointing the profile of the rotation disk more difficult.

It can be concluded that the DSLR method is probably not the best for accurate measurements. First, the deflections are rather small, meaning that the errors in calibration and data extraction reduce the fidelity of the method. Second, due to the manual way of extracting data, the results have a human error factor in them that affects which points are chosen and could possibly be biased. Instead, a more automated process is recommended with fixed target positions that are determined prior to the experiment, just as it is done in the photogrammetry method. And last, the speed of the camera, quality of the photos, and the surroundings make a significant difference when post-processing the results, hence making the test quite hardware- and condition-dependent. Nevertheless, the method is still considered good enough to get a rough estimation of these kinds of deflections for validation of an FE simulation. One improvement for future tests of this kind would be to mark a spot on the blades so that the data can be extracted from exact places. This was not done in this test because the same blades were going to be used for other tests (thus the desire to not create any permanent changes to them), but also due to the same external trigger and target problems that occurred in the tailored photogrammetry method.

Regarding the photogrammetry, it can be concluded that the method is more suitable for deflection measurements than the DSLR method, primarily because the number of sources of error is limited and higher precision is possible. That is not to say that the method is perfect. It still has some artifacts that could be excluded if there was time to improve the methodology. The main improvement would be to actually receive a trigger pulse for the cameras at the exact same azimuth for all rotation speeds. That way the targets position could be steadier and hopefully reduce the noise in the measurements that made the change in pitch angle computations more challenging.

Another issue that should be pointed out is the use of targets. In this approach, quite a few targets were used since it was not known which points would be needed further on in the analysis. More targets, even though they are small, might affect the stiffness and aerodynamic properties of the blade, and with the small margins of errors, it might add up to the overall error. Depending on where the pitch needs to be calculated, the amount of targets could be reduced or even changed to laser grid targets that have less effect on the blades. Another aspect is blade quality and balance. In this study it was desired to tell the two blades on each propeller apart, so one of the blades had one or two extra targets. Afterwards, it was clear that this caused a small imbalance in the cheaper DJI propellers as one side had a slightly larger deflection than the other. To avoid that in the future, it is recommended to have the same number of targets but color at least one of them with a marker so that it will not reflect the strobe light, hence showing a different

amount of targets in the photos. Another option is to have different patterns on the two blades, but that could also cause small differences in the balance.

One last comment on the photogrammetry method would be improvements of calibration. Even though the calibration board was solid and rather exact, there were some practical difficulties of fastening it as planar as possible against the motor. Although deformations are very small, this might have some effect on the end results. To improve the fidelity further, it could be beneficial to compensate for any lens distortion that might be present, especially at the borders of the photogrammetry. This was unfortunately thought of too late, and there was not enough time to include it in the post-processing.

If the VSTARS system can be updated to allow for tracking the targets in larger regions of interest, or if it can be incorporated with a 1-per-revolution trigger system, the method shows good potential for being used for these types of measurements. The high-fidelity, good precision, simple measurement setup, along with live results, is clearly beneficial. The main advantage would be saving post-processing time, as the results are very time consuming for the tailored method if more measurements are needed to get statistical samples.

The theory used in this study, as was as pointed out in the beginning, was developed for helicopters. Therefore, the validity region of this theory should be considered. The theory is clearly applicable to helicopters but neither Johnson [26] nor Leishman [25] mention its validity for smaller applications. One variation is that the helicopter blades usually have hinges and swashplates whereas multicopter rotors do not. The blades of multicopters are also much smaller and are rigidly attached to the hub, while the geometry itself is more complex. Nevertheless, the general equations of motions are still valid, but the authors use several approximations, such as constant chord length, symmetric airfoil, and constant rate of change in twist, to simplify the equations and get analytical equations. The question is then how valid are these simplifications for the geometry and properties of multicopter blades that have neither of those characteristics. In the presented case, the compensation for the cambered airfoils will only be as good as the airfoils of the CAD model that were studied in XFOIL. Yet another problem is the very low Reynolds number. It is usually considered problematic when it is below 100,000, and in this case it was as low as 30,000 for the lower RPM. This clearly affects the angle of attack at zero lift that is needed for the coning angle and the lift distribution. Also, the lift theory might have its limits for such low Reynolds numbers, therefore possibly resulting in the lower theoretical lift. The nondimensional frequency was, for example, also approximated from the helicopter theory. This is clearly not the perfect approximation, but it gives a range of where the results should be to be used as a guideline. Another aspect is that the theory neglects blade weight moments and tip losses that are present in the real cases of blade motion. There is theory that takes these effects into account, but it was considered an acceptable assumption due to the low weight and fast tip speeds of the multicopter blades. It is therefore possible that a more exact model could have been better to use, however the complex geometry and unknown mass distribution of the blades made such calculations too complicated. Therefore, it should be noted, the theory is not perfectly adjusted for multicopter UAS.

Only one model was tested for the FEA simulations. It was considered to include the main forces acting on the blades as well as the proper boundary conditions. However, as could be seen in the results, the models over predicted the out-of-plane deflection and always resulted in a positive change in pitch. This was not observed in the photogrammetry measurements, even though the theoretical lift was lower than the output from the performance measurements from the DSLR method in both cases. Whether that has to do with the validity of the lift theory or the parameters extracted from the CAD models is hard to determine without further testing. It should, nevertheless, be noted that the model overestimates the out-of-plane

deflection even more with this in mind. On the other hand, changing the model to a large deflection test was not considered valid since the deformations without it were well within the bounding box of the CAD models.

Another aspect to keep in mind is the choice of material properties for the DJI propellers. Sources of error from the material tests performed to estimate the material properties could exist and affected the outcome. One clear problem was the nonsymmetric geometry where the cross sections changed. The tabs were another problem, as the geometry demanded usage of more adhesive material just to fill out the space and get parallel tabs. If the adhesive did not fasten as well as hoped for to the test specimen, due to problems with thermoplastic and thermoset bonding, it might also add to a potential error. Even though great care was put into avoiding sources of errors, all of these things might affect the tensile test, which might have resulted in some small sliding or even shearing if everything was not perfectly aligned. That, in turn, could explain the lower than expected elastic modulus of 6.5 GPa as the deformation would be higher for a smaller load. If that is the case, it is not possible to determine the true elastic modulus other than to say that it most likely has a lower bound of 6.5 GPa, but is closer to the 9.5 GPa predicted by the simulations.

In the case of the carbon fiber, the model had a large error when predicting 2.5 mm out-of-plane deflection while it only was 1.1 mm in the photogrammetry results. Two possible sources of error are the estimated material properties and the software itself. It is fairly well known that ANSYS is not ideal for modeling 3D composites with such a complex 3D geometry. Even though element orientation was applied, the 3D structure of a plain composite weave might not have translated as well as it was hoped for, possibly due to the simplification where the in-plane and out-of-plane material properties were defined.

The used model hence overestimates the out-of-plane deflection and overestimates the change in pitch to a positive value. An improvement would clearly be to perform a CFD analysis to see if the calculated theoretical lift contains errors and to use a smoother lift distribution. Unfortunately, due to lack of knowledge within that area and the limited time frame of the project, such an analysis was not performed. It is also possible that an extended material model or another non-dedicated commercial software could give better results for the carbon fiber blades. If that was the case, then more enthusiasts with access to such non-dedicated software could test their blades fairly easily. Otherwise it has to be said that dedicated software is most likely more desirable for simulations like these and should be tested to see if it can predict the deformations of these geometrically challenging rotors.

To summarize this evaluation, it is clear that the methods and theory for analyzing rotor blades need revision and improvement. All the drawbacks of the models that were discussed herein point to that conclusion. It is also recommended to investigate how the blades behave in modes other than hover, such as forward flight. That way, the structural properties can be better understood. Hopefully such a test could then take into account the proposed improvements in the methods and obtain even more reliable results.

Another clear next step in analyzing these rotor blades would be to try out some of the new dedicated software that include 3D structural analysis, such as X3D. To get a good correspondence, the code should be tested in a static load mode and in the built-in hover mode, which could then to be compared to the results obtained in this report. Yet, it must be pointed out that due to the early stage of development the X3D software, the fidelity of the code for different applications, and the implementation of the different flight modes might still have some shortcomings. Nevertheless, the code shows good fidelity on the configurations that have been tested, and it is continuously being tested and improved. It is consequently not too bold to say that once it is complete, it will clearly contribute in the field of rotorcraft analysis and, together with similar codes, provide an easy and reasonably cheap way of evaluating a product in the early stages of its development. That way multicopters with dedicated field of use could have improved

performance and be optimized to their purpose. Moreover, the general operational envelope of UAS could be increased, hence providing better products. As said in the beginning, multicopter UAS have some clear advantages and can be very helpful in several aspects including projects where medicine and supplies need be delivered to isolated catastrophe areas or to reduce use of fossil fuels in fast deliveries. The benefits for society are thus great if used correctly.

8. Conclusion

In this report, the relation between rotor blade deformation and RPM has been studied in hover mode for two types of commercially available UAS multicopter propellers. It can be concluded that performing measurements on such small, fast moving, and geometrically complicated parts is challenging and easily gives rise to problems such as accuracy and which methods could be applied. The deformations are very small compared to the geometry of the product, meaning that high precision and exclusions of as many numerical and human errors as possible are necessary. One of the main conclusions of this study is that photogrammetry is the preferred method, as it offers more reliability and less sources of error, while the DSLR method could possibly be used for estimating the magnitude of the out-of-plane deflection. However, to get higher fidelity of the change in pitch angle results, the photogrammetry methods need improvement in the form of target choice, better camera triggers for measurements at consistent azimuth, field of view adjustment, and calibration.

For the plastic DJI Phantom 3 propellers, the out-of-plane deflection from both measurements and theory shows a linear to negative quadratic relation for a sweep between 2500 and 8500 RPM. The maximum deflection at 7500 RPM was around 3.7 mm for both measurement types resulting in a coning angle of about 1.6 degrees, which is fairly comparable to the theoretical value of 1.75 degrees. The change in pitch showed a tendency of decreasing angle. For the carbon fiber composite T-motor 15x5 propeller, the out-of-plane deflection showed a linear to positive quadratic relation, but more scatter and errors were present in the measurements. The maximum out-of-plane deflection at 5000 RPM was about 1.1 mm as found by the photogrammetry, which gives a coning angle that is just slightly lower than the theoretical angle. The change in pitch kept an almost constant angle.

The simulation showed that the model used was not detailed enough to provide reliable results. The theory underestimated the lift and still gave an out-of-plane deflection that was slightly bigger than the measured results. The change in pitch was overestimated as well and resulted in an increased pitch angle in all cases, which is the opposite of the trend shown in the photogrammetry results. For the DJI Phantom 3 propellers, the results were a bit more consistent with the measured deflection, at least for one of the material models. A more thorough model with a CFD analysis is needed to obtain more reliable results, and preferably also use software dedicated to rotorcraft analysis with the capability of performing high fidelity FEA and CFD coupled analyses.

References

[1] Amazon.com, Inc.: Amazon Prime Air. Available: http://www.amazon.com/b?node=8037720011. [Accessed Feb. 10, 2016].

[2] Eadicicco, L.: Amazon Reveals New Details About Drone Deliveries. Time, Jan. 19, 2016.

[3] Federal Aviation Administration (FAA), Department of Transportation (DOT), Operation and Certification of Small Unmanned Aircraft Systems.

[4] Anon.: T-MOTOR, 2013. Available: http://www.rctigermotor.com/. [Accessed March 1, 2016].

[5] Gil, L.: New Cork-Based Material and Applications. Materials, vol. 8, no. 2, pp. 625–637, 2015.

[6] Cox, J.; Burdette, D.; Shaffer, C.; and Zabihian, F.: Lighter Than Air UAV. ASEE 2014 Zone I Conference, Bridgport, CT, 2014.

[7] Patkar, U.; Datta, S.; Majumder, S.; Ray, D.; Char, S.; and Majumder, M: Studies on Effect of Basic Manuvering Operations on Quadcopters Thrust Generated. International Conference on Robotics, Biomimetics, Intelligent Computational Systems, Yogyakarta, Indonesia, 2013.

[8] Pounds, P.; Mohoney, R.; and Corke, P.: Modelling and Control of a Quad-Rotor Robot. Control Engineering Practice, vol. 18, no. 7, p. 691–699, 2010.

[9] Huang, H; Hoffmann, G. M.; Waslander, S. L.; and Tomlin, C. J.: Aerodynamics and Control of Autonomous Quadrotor Helicopters in Aggressive Maneuvering. 2009 IEEE International Conference on Robotics and Automation, Kobe, Japan, 2009.

[10] Hoffmann, G. M.; Huang, H.; Waslander, S. L.; and Tomlin, C. J.: Quadrotor Helicopter Flight Dynamics and Control: Theory and Experiment. AIAA Guidance, Navigation and Control Conference and Exhibit, Hilton Head, SC, 2007.

[11] Pereira, J. L.: Hover and Wind-Tunnel Testing of Shrouded Rotors for Improved Micro Air Vehicle Design. 09 08 2008. Available: http://drum.lib.umd.edu/handle/1903/8752. [Accessed March 10, 2016].

[12] Brandt, J. B. and Selig, M. S.: Propeller Performance Data at Low Reynolds Numbers. 49th AIAA Aerospace Sciences Meeting, Orlando, FL, 2011.

[13] Russell, C.; Jung, J.; Willink, G.; and Glasner, B.: Wind Tunnel and Hover Performance Test Results for Multicopter UAS Vehicles. 72nd AHS Annual Forum, Palmdale, FL, 2016.

[14] Ormiston, R. A. and Hodges, D. H.: Linear Flap-Lag Dynamics of Hingeless Helicopter Rotor Blades in Hover. Journal of The American Helicopter Society, vol. 17, no. 2, pp. 2–14, 1972.

[15] Hodges, D. H.: Review of Composite Rotor Blade Modeling. AIAA Journal, vol. 28, no. 3, pp. 561–565, 1990.

[16] Yuan, K. A. and Freidmann, P. P.: Aeroelasticity and Structural Optimization of Composite Helicpoter Rotor Blades With Swept Tips. NASA CR 4665, Langley Research Center, Hampton, VA, 1995.

[17] W. Staruk; I. Chopra; and A. Datta: Three-Dimensional CAD-Based Structural Modeling for Next Generation Rotor Dynamic Analysis. AHS 70th Annual Forum, Montreal, Québec, Canada, 2014.

[18] Sivaneri, N. T. and Chopra, I.: Dynamic Stability of a Rotor Blade Using Finite Element Analysis. AIAA Journal, vol. 20, no. 5, pp. 716–723, 1982.

[19] Hodges, D. H. and Yu, W.: A Rigorous, Engineer-Friendly Aproach for Modelling Realistic Composite Rotor Blades. Wind Energy, vol. 10, no. 2, pp. 179–193, 2007.

[20] Friedmann, P. P.; Glaz, B.; and Palacios, R.: A Moderate Deflection Composite Helicopter Rotor Blade Model With an Improved Cross-Sectional Analysis. International Journal of Solids and Structures, vol. 46, pp. 2186–2200, 2009.

[21] Johnson, W.: Rotorcraft Dynamics Model for a Comprehensive Analysis. The American Helicopter Society 54th Annual Forum, Washington, DC, 1998.

[22] Datta, A.: X3D – A 3D Solid Finite Element Multibody Dynamic Analysis for Rotorcraft. American Helicopter Society Technical Meeting on Aeromechanics Design for Vertical Lift, San Francisco, CA, 2016.

[23] Staruk, W.; Chopra, I.; and Datta, A.: Coupled Aerodynamics and 3-D Structural Dynamics of the Tilt Rotor Aeroacoustic Model (TRAM) Proprotor. AHS International Technical Meeting on Aeromechanics Design for Vertical Lift, San Francisco, CA, 2016.

[24] Anon.: DJI – The World Leader in Camera Drones/Quadcopters for Aerial Photography. 2016. Available: http://www.dji.com/. [Accessed March 1, 2016].

[25] Leishman, J. G.: Principles of Helicopter Aerodynamics, USA: Cambridge University Press, 2000.

[26] Johnson,W.: Rotorcraft Aermechanics, USA: Cambrige University Press, 2013.

[27] Tummers, B.: DataThief III. 2016. Available: http://www.datathief.org/.

[28] Anon.: Geodetic, Inc. Jack Marlow, 2016. Available: http://www.geodetic.com/. [Accessed April 5, 2016].

[29] MatWeb, LLC: Online Materials Information Resource - MatWeb. 2016. Available: http://www.matweb.com/. [Accessed May 20, 2016].

[30] Bijsterbosch, H. and Gaymans, R. J.: Polyamide 6 Long Glass Fiber Injection Moldings. Polymer Composites, vol. 16, no. 5, pp. 363–369, 1995.

[31] Anon.: Engineering Materials. Available: http://www.engineeringtoolbox.com/engineering-materials-properties-d_1225.html. [Accessed June 20, 2016].

[32] U.S. Department of Defense: Military Handbook - MIL-HDBK-17-1F: Composite Materials Handbook, Volume 2. Polymere Matrix Composites Material Properties. U.S. Department of Defense, 2002.

[33] Anon.: Cork - MakeItFrom.com. 08 05 2016. Available: http://www.makeitfrom.com. [Accessed June 10, 2016].

[34] Mital, S. K.; Murthy, P. L.; and Chamis, C. C.: Simplified Micromechanics of Plain Weave Composites. NASA TM 107165, Mar. 1996.

[35] Drela, M.: Xfoil Subsonic Airfoil Development System. Available: web.mit.edu/drela/Public/web/xfoil. [Accessed 2016].

Appendix A—FEA Convergence Study

Convergence studies were performed for the finite element (FE) studies. All studies show how the inverse of the number of elements corresponds to chosen displacements with an interpolated value from the last measured point to an infinite number of elements for which a mesh error is estimated. Figure 29 shows the convergence study for the static bending test for the DJI propeller and yields an error of < 1 percent. Figure 30 shows the convergence study for the hover simulation for the DJI propeller, and Figure 31 depicts the study for the T-motor propeller. The corresponding errors are 1.2 and 1.8 percent, respectively.

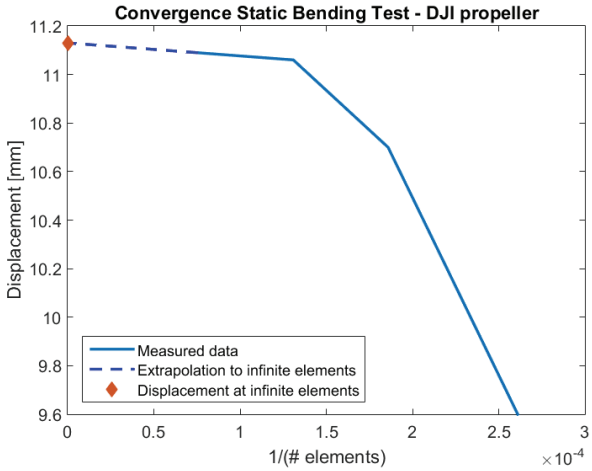

Figure 29: Convergence study of static bending test—DJI Phantom 3 propeller.

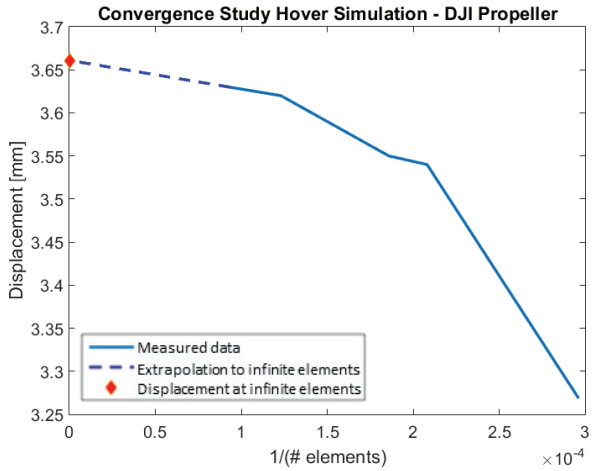

Figure 30: Convergence study of hover simulation—DJI Phantom 3 propeller.

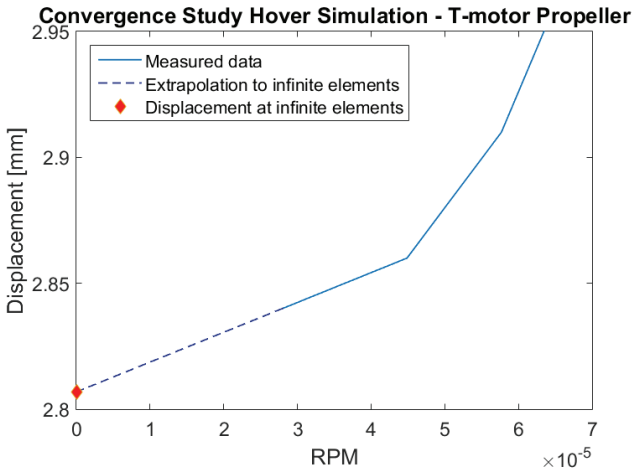

Figure 31: Convergence study of hover simulation—T-motor 15x5 propeller.

Appendix B—Numerical Results, DSLR Camera Measurements

The following numerical results from the DSLR camera measurements include both the out-of-plane deflection and the corresponding coning angle for comparison with analytical solutions. Table 9 presents the deflection and the coning angle for the single test of the carbon fiber T-motor blade. Table 10 present the individual results from the plastic DJI Phantom 3 propeller 1 done during three separate test runs. Table 11 and Table 12 show the results from the third and final test run for the five studied DJI propellers.

Table 9: Deflection [mm] and coning angle [deg] results from DSLR camera test for T-motor propeller.

RPM	2000	2500	3000	3500	4000	4500	5000
Deflection	0.22	0.46	0.02	1.44	1.39	1.62	1.87
Coning Angle	0.11	0.22	0.01	0.69	0.67	0.77	0.89

Table 10: Deflection [mm] and coning angle [deg] results from DSLR camera test for DJI propeller 1.

RPM	Run 1 – Deflection	Run 2 – Deflection	Run 3 – Deflection	Run 1 – Coning Angle	Run 2 – Coning Angle	Run 3 – Coning Angle
2500	0.10	0.59	0.89	0.05	0.28	0.42
3000	1.14	0.73	1.18	0.55	0.35	0.56
3500	1.43	1.32	1.48	0.68	0.63	0.71
4000	1.91	1.46	1.62	0.91	0.70	0.78
4500	2.19	2.05	2.36	1.05	0.98	1.13
5000	2.38	2.49	2.36	1.14	1.19	1.13
5500	2.38	2.63	2.66	1.14	1.26	1.27
6000	2.77	2.78	2.95	1.32	1.33	1.41
6500	2.29	3.07	3.40	1.09	1.47	1.62
7000	3.05	3.36	3.40	1.46	1.61	1.62
7500	2.86	3.51	3.69	1.37	1.68	1.76
8000	3.43	3.51	3.99	1.64	1.68	1.90
8500	3.53	3.80	3.99	1.68	1.81	1.90

Table 11: Out-of-plane deflection [mm] results from DSLR camera test for DJI propellers 1–5.

RPM	Prop 1	Prop 4	Prop A	Prop B	Prop C	Mean	Standard Mean Error
2500	0.89	1.33	0.59	0.42	0.43	**0.73**	**0.17**
3000	1.18	1.62	0.59	1.16	0.73	**1.06**	**0.18**
3500	1.48	1.92	0.15	1.61	0.88	**1.21**	**0.31**
4000	1.62	2.07	1.48	1.75	1.47	**1.68**	**0.11**
4500	2.36	2.66	1.77	2.19	1.91	**2.18**	**0.16**
5000	2.36	2.95	2.07	2.63	2.35	**2.47**	**0.15**
5500	2.66	3.25	2.51	2.92	2.49	**2.77**	**0.14**
6000	2.95	3.54	2.66	3.21	2.79	**3.03**	**0.16**
6500	3.40	3.84	2.81	3.50	2.93	**3.30**	**0.19**
7000	3.40	4.14	2.95	3.51	3.23	**3.44**	**0.20**
7500	3.69	4.28	3.40	3.80	3.48	**3.73**	**0.16**
8000	3.99	4.43	3.40	4.23	3.66	**3.94**	**0.19**
8500	3.99	4.58	3.69	4.38	3.81	**4.08**	**0.17**

Table 12: Coning angle [deg] results from DSLR camera test for DJI propellers 1–5.

RPM	Prop 1	Prop 4	Prop A	Prop B	Prop C	Mean	Standard Mean Error
2500	0.42	0.63	0.28	0.20	0.21	**0.35**	**0.08**
3000	0.56	0.78	0.28	0.56	0.35	**0.51**	**0.09**
3500	0.71	0.92	0.07	0.77	0.42	**0.58**	**0.15**
4000	0.78	0.99	0.71	0.84	0.70	**0.80**	**0.05**
4500	1.13	1.27	0.85	1.04	0.91	**1.04**	**0.08**
5000	1.13	1.41	0.99	1.25	1.12	**1.18**	**0.07**
5500	1.27	1.55	1.20	1.39	1.19	**1.32**	**0.07**
6000	1.41	1.69	1.27	1.53	1.33	**1.45**	**0.08**
6500	1.62	1.83	1.34	1.67	1.40	**1.57**	**0.09**
7000	1.62	1.97	1.41	1.67	1.54	**1.64**	**0.09**
7500	1.76	2.04	1.62	1.81	1.66	**1.78**	**0.07**
8000	1.90	2.11	1.62	2.02	1.75	**1.88**	**0.09**
8500	1.90	2.18	1.76	2.09	1.82	**1.95**	**0.08**

Appendix C—Numerical Results, Photogrammetry

The numerical out-of-plane deflection results at the tip from each blade test acquired with the help of photogrammetry are shown in Table 13 to Table 18 below. Table 13 shows the results for the single T-motor blade that was tested. Next Table 14 to Table 18 correspond to DJI Phantom 3 propellers number 1, 4, A, B, and C respectively. Table 19 to Table 24 shows the results from the change in pitch in the same order as the displacement table. The pitch angle change was calculated at the second target pair, more precisely targets at leading edge and trailing edge about 15 mm from the tip.

Table 13: Results of out-of-plane deflection at leading edge and tip of blade from photogrammetery test for T-motor blade.

RPM	Take 1	Take 2	Take 3	Take 4	Take 5	Mean	Standard Mean Error
2000	0.19	-0.18	0.20	-0.89	-0.70	**-0.28**	**0.20**
2500	0.10	0.08	0.15	0.15	-	**0.12**	**0.02**
3000	0.77	0.77	0.77	-2.83	0.70	**0.04**	**0.64**
3500	0.64	0.70	0.73	0.69	0.69	**0.69**	**0.01**
4000	0.46	0.50	0.40	0.53	0.63	**0.51**	**0.03**
4500	0.48	0.46	0.43	0.44	0.42	**0.44**	**0.01**
5000	1.08	1.14	1.12	1.13	1.15	**1.12**	**0.01**
5500	1.24	1.31	1.41	1.39	1.38	**1.35**	**0.03**

Table 14: Results of out-of-plane deflection at leading edge and tip of blade from photogrammetery test for DJI Phantom 3 propeller 1.

RPM	Take 1	Take 2	Take 3	Take 4	Take 5	Take 6	Take 7	Take 8	Mean	Standard Mean Error
2500	0.86	0.83	0.87	0.81	0.86	0.82	0.86	0.87	**0.85**	**0.01**
3000	1.23	1.21	1.32	1.27	1.29	1.26	1.17	1.25	**1.25**	**0.02**
3500	1.54	1.44	1.35	1.45	1.39	1.53	1.47	1.38	**1.44**	**0.02**
4000	-	-	-	-	-	-	-	-	**-**	**-**
4500	2.23	2.30	2.27	2.25	2.25	2.37	2.48	2.48	**2.33**	**0.03**
5000	2.62	2.66	2.68	2.62	2.64	2.63	2.53	2.59	**2.62**	**0.02**
5500	2.94	2.96	2.97	2.93	2.95	3.00	2.96	2.96	**2.96**	**0.01**
6000	3.23	3.25	3.24	3.15	3.10	3.16	3.11	3.23	**3.18**	**0.02**
6500	3.14	3.16	3.21	3.19	3.15	3.14	3.16	3.09	**3.15**	**0.01**
7000	3.60	3.60	3.60	3.68	3.71	3.72	3.62	3.68	**3.66**	**0.02**
7500	3.48	3.36	3.42	3.43	3.46	3.51	3.40	3.42	**3.43**	**0.02**

Table 15: Results of out-of-plane deflection at leading edge and tip of blade from photogrammetery test for DJI Phantom 3 propeller 4.

RPM	Take 1	Take 2	Take 3	Take 4	Take 5	Take 6	Take 7	Take 8	Mean	Standard Mean Error
2500	0.84	0.87	0.87	0.92	0.85	0.83	0.82	0.82	**0.85**	**0.01**
3000	1.19	1.14	1.14	1.17	1.05	1.17	1.12	1.15	**1.14**	**0.01**
3500	1.38	1.41	1.32	1.35	1.32	1.36	1.34	1.41	**1.36**	**0.01**
4000	1.80	1.79	1.88	1.79	1.86	1.77	1.79	1.89	**1.82**	**0.02**
4500	2.11	2.07	2.11	2.08	2.08	2.08	2.15	2.21	**2.11**	**0.02**
5000	2.31	2.35	2.39	2.32	2.26	2.31	2.26	2.29	**2.31**	**0.02**
5500	2.97	3.00	2.90	2.96	2.92	2.96	2.94	2.97	**2.95**	**0.01**
6000	2.80	2.89	2.83	2.87	2.87	2.87	2.81	2.85	**2.85**	**0.01**
6500	3.07	3.00	2.99	3.08	3.06	3.14	3.09	3.03	**3.06**	**0.02**
7000	3.15	3.12	3.15	3.12	3.17	3.14	3.17	3.20	**3.15**	**0.01**
7500	3.51	3.46	3.43	3.46	3.45	3.55	-	-	**3.48**	**0.02**

Table 16: Results of out-of-plane deflection at leading edge and tip of blade from photogrammetery test for DJI Phantom 3 propeller A.

RPM	Take 1	Take 2	Take 3	Take 4	Take 5	Take 6	Take 7	Take 8	Mean	Standard Mean Error
2500	0.88	0.86	0.77	0.86	0.82	0.84	0.74	0.81	**0.82**	**0.02**
3000	1.13	1.11	1.07	1.13	1.21	1.10	1.13	1.13	**1.13**	**0.01**
3500	1.45	1.35	1.40	1.46	1.38	1.39	1.41	1.46	**1.41**	**0.01**
4000	1.89	1.74	1.82	1.76	1.76	1.69	1.7	1.72	**1.76**	**0.02**
4500	2.58	2.54	2.53	2.54	2.57	2.53	2.55	2.56	**2.55**	**0.01**
5000	2.44	2.46	2.41	2.40	2.43	2.42	2.49	2.44	**2.43**	**0.01**
5500	2.96	2.90	3.01	2.97	2.95	2.97	2.96	2.95	**2.96**	**0.01**
6000	2.86	2.91	2.98	2.94	2.96	2.93	2.96	2.88	**2.93**	**0.01**
6500	3.32	3.32	3.32	3.35	3.30	3.40	3.40	3.37	**3.35**	**0.01**
7000	3.49	3.46	3.51	3.45	3.43	3.48	3.39	3.46	**3.46**	**0.01**
7500	3.83	3.77	3.77	-	-	-	-	-	**3.79**	**0.02**

Table 17: Results of out-of-plane deflection at leading edge and tip of blade from photogrammetry test for DJI Phantom 3 propeller B.

RPM	Take 1	Take 2	Take 3	Take 4	Take 5	Take 6	Take 7	Take 8	Mean	Standard Mean Error
2500	0.82	0.76	0.80	0.70	0.81	0.80	0.83	0.82	**0.79**	**0.01**
3000	1.13	1.06	1.03	0.98	1.04	1.06	1.05	1.15	**1.06**	**0.02**
3500	1.42	1.39	1.45	1.60	1.58	1.44	1.47	1.42	**1.47**	**0.03**
4000	1.83	1.82	1.82	1.91	1.80	1.92	1.73	1.89	**1.84**	**0.02**
4500	-	-	-	-	-	-	-	-	**-**	**-**
5000	2.58	2.63	2.55	2.55	2.58	2.55	2.57	2.67	**2.58**	**0.02**
5500	2.99	3.01	2.96	2.93	2.92	2.93	2.97	2.96	**2.96**	**0.01**
6000	2.76	2.85	2.80	2.83	2.71	2.70	2.78	2.62	**2.76**	**0.03**
6500	3.52	3.48	3.53	3.42	3.48	3.50	3.54	-	**3.50**	**0.01**
7000	3.73	3.71	3.74	3.77	3.70	3.70	3.74	3.73	**3.73**	**0.01**
7500	3.94	3.99	3.97	3.90	4.01	4.00	3.99	4.01	**3.98**	**0.01**

Table 18: Results of out-of-plane deflection at leading edge and tip of blade from photogrammetry test for DJI Phantom 3 propeller C.

RPM	Take 1	Take 2	Take 3	Take 4	Take 5	Take 6	Take 7	Take 8	Mean	Standard Mean Error
2500	-	-	-	-	-	-	-	-	**-**	**-**
3000	1.31	1.37	1.35	1.35	1.39	1.35	1.30	1.27	**1.34**	**0.01**
3500	1.52	1.52	1.53	1.46	1.49	1.43	1.45	1.46	**1.48**	**0.01**
4000	1.87	1.90	1.92	1.86	1.89	1.90	1.88	1.91	**1.89**	**0.01**
4500	2.14	2.09	2.16	2.21	2.21	2.23	2.19	2.20	**2.18**	**0.03**
5000	2.32	2.28	2.25	2.35	2.31	2.29	2.30	2.33	**2.30**	**0.01**
5500	2.73	2.75	2.66	2.69	2.65	2.67	2.69	2.76	**2.70**	**0.01**
6000	-	-	-	-	-	-	-	-	**-**	**-**
6500	3.20	3.21	3.28	3.18	3.24	3.17	3.23	3.22	**3.22**	**0.01**
7000	3.17	3.10	3.11	3.15	3.14	3.28	3.14	3.17	**3.16**	**0.02**
7500	3.78	3.80	3.75	-	-	-	-	-	**3.78**	**0.01**

Table 19: Results of change in pitch angle at leading edge and 15 mm from the tip of the blade aqcuired with photogrammetery test for T-motor propeller.

RPM	Take 1	Take 2	Take 3	Take 4	Take 5	Mean	Standard Mean Error
2000	1.16	-0.41	1.54	0.14	-0.37	**0.41**	**0.40**
2500	0.01	0.41	-0.34	0.08	0.16	**0.06**	**0.12**
3000	0.09	0.21	0.08	0.04	0.11	**0.11**	**0.03**
3500	0.21	0.14	0.02	0.04	-0.01	**0.08**	**0.04**
4000	0.10	0.06	0.12	0.13	-0.02	**0.08**	**0.03**
4500	-0.07	-0.03	0.10	0.22	0.10	**0.06**	**0.05**
5000	0.13	0.28	0.18	0.20	0.27	**0.21**	**0.03**
5500	0.15	0.30	0.21	0.10	0.04	**0.16**	**0.04**

Table 20: Results of change in pitch angle at leading edge and 15 mm from the tip of the blade acquired with photogrammetry test for DJI Phantom 3 propeller 1.

RPM	Take 1	Take 2	Take 3	Take 4	Take 5	Take 6	Take 7	Take 8	Mean	Standard Mean Error
2500	-0.40	-0.27	-0.03	-0.20	-0.07	-0.43	-0.20	-0.13	**-0.22**	**0.05**
3000	-0.07	-0.06	0.16	-0.11	0.08	-0.05	0.24	0.12	**0.04**	**0.05**
3500	-0.21	-0.26	-0.64	-0.09	-0.45	-0.41	-0.22	-0.40	**-0.34**	**0.06**
4000	-	-	-	-	-	-	-	-	**-**	**-**
4500	-0.18	-0.35	-0.38	-0.48	-0.41	-0.41	-0.54	-0.54	**-0.41**	**0.04**
5000	-0.55	-0.41	-0.38	-0.74	-0.80	-0.47	-0.63	-0.48	**-0.56**	**0.06**
5500	-0.35	-0.44	-0.44	-0.39	-0.34	-0.46	-0.41	-0.35	**-0.40**	**0.02**
6000	-0.20	-0.61	-0.54	-0.50	-0.56	-0.60	-0.31	-0.52	**-0.48**	**0.05**
6500	-0.53	-0.83	-0.85	-0.61	-0.70	-0.63	-0.77	-0.72	**-0.70**	**0.04**
7000	-0.84	-0.74	-0.81	-0.76	-1.06	-0.69	-0.64	-0.95	**-0.81**	**0.05**
7500	-0.72	-0.82	-0.93	-0.68	-0.84	-0.74	-0.84	-0.74	**-0.79**	**0.03**

Table 21: Results of change in pitch angle at leading edge and 15 mm from the tip of the blade acquired with photogrammetry test for DJI Phantom 3 propeller 4.

RPM	Take 1	Take 2	Take 3	Take 4	Take 5	Take 6	Take 7	Take 8	Mean	Standard Mean Error
2500	0.29	0.40	0.27	0.02	0.19	0.02	-0.03	0.17	**0.17**	**0.05**
3000	-0.11	-0.27	-0.04	-0.04	-0.01	0.16	-0.11	0.08	**-0.04**	**0.05**
3500	-0.57	-0.28	-0.56	-0.17	-0.24	-0.46	-0.28	-0.32	**-0.36**	**0.05**
4000	-0.52	-0.51	-0.51	-0.38	-0.54	-0.55	-0.55	-0.49	**-0.51**	**0.02**
4500	-0.44	-0.62	-0.47	-0.77	-0.67	-0.59	-0.66	-0.85	**-0.63**	**0.05**
5000	-0.06	-0.28	-0.25	-0.27	-0.04	0.08	-0.29	-0.31	**-0.18**	**0.05**
5500	-0.33	-0.63	-0.61	-0.83	-0.70	-0.90	-0.62	-0.52	**-0.65**	**0.06**
6000	-0.56	-0.24	-0.23	-0.25	-0.01	-0.13	-0.10	-1.63	**-0.39**	**0.19**
6500	-0.63	-0.53	-0.55	-0.92	-0.77	-0.92	-0.89	-0.59	**-0.73**	**0.06**
7000	-0.47	-0.58	-0.71	-0.46	-0.32	-0.74	-0.63	-0.72	**-0.58**	**0.05**
7500	-0.28	-0.79	-0.58	-0.91	-0.53	-0.48	-	-	**-0.60**	**0.09**

Table 22: Results of change in pitch angle at leading edge and 15 mm from the tip of the blade acquired with photogrammetry test for DJI Phantom 3 propeller A.

RPM	Take 1	Take 2	Take 3	Take 4	Take 5	Take 6	Take 7	Take 8	Mean	Standard Mean Error
2500	0.53	0.22	0.21	0.11	-0.09	0.45	0.09	0.09	**0.20**	**0.07**
3000	0.26	0.09	-0.03	0.08	0.17	0.37	0.29	0.25	**0.19**	**0.05**
3500	-0.27	-0.46	-0.29	-0.42	-0.37	-0.40	-0.34	-0.50	**-0.38**	**0.03**
4000	-0.03	0.11	-0.23	-0.38	-0.27	0.02	-0.07	-0.03	**-0.11**	**0.06**
4500	-0.18	0.10	-0.14	0.08	0.10	0.14	0.02	-0.11	**0.00**	**0.05**
5000	-0.45	-0.14	-0.17	-0.32	-0.25	0.08	-0.14	-0.04	**-0.18**	**0.06**
5500	-0.20	-0.15	-0.21	-0.08	-0.12	-0.01	-0.20	-0.36	**-0.17**	**0.04**
6000	-0.68	-0.44	-0.24	-0.43	-0.65	-0.35	-0.53	-0.36	**-0.46**	**0.05**
6500	-0.58	-0.39	-0.40	-0.49	-0.65	-0.67	-0.71	-0.21	**-0.51**	**0.06**
7000	-0.37	-0.60	-0.30	-0.29	-0.56	-0.61	-0.47	-0.38	**-0.45**	**0.05**
7500	-0.32	-0.36	-0.45	-0.59	-	-	-	-	**-0.43**	**0.06**

Table 23: Results of change in pitch angle at leading edge and 15 mm from the tip of the blade acquired with photogrammetry test for DJI Phantom 3 propeller B.

RPM	Take 1	Take 2	Take 3	Take 4	Take 5	Take 6	Take 7	Take 8	Mean	Standard Mean Error
2500	0.03	-0.39	0.02	-0.21	0.12	-0.25	-0.30	-	**-0.14**	**0.07**
3000	-0.26	-0.08	-0.51	-0.29	-0.09	-0.10	-0.12	-0.43	**-0.23**	**0.06**
3500	-0.02	-0.15	0.12	-0.07	-0.14	-0.03	-0.20	-0.08	**-0.07**	**0.04**
4000	-0.42	-0.46	-0.30	-0.41	-0.37	-0.50	-0.49	-0.12	**-0.38**	**0.04**
4500	-	-	-	-	-	-	-	-	**-**	**-**
5000	-0.03	-0.02	-0.10	-0.17	0.13	-0.12	0.01	0.01	**-0.04**	**0.03**
5500	1.84	1.93	1.83	1.64	1.85	1.70	1.87	1.72	**1.80**	**0.04**
6000	-0.17	-0.52	-0.42	-0.33	-0.33	-0.44	-0.78	-0.41	**-0.43**	**0.06**
6500	-0.44	-0.35	-0.24	0.80	-0.72	-0.49	-0.54	-	**-0.28**	**0.19**
7000	-0.47	-0.59	-0.24	-0.36	-0.11	-0.44	-0.26	-0.08	**-0.32**	**0.06**
7500	-0.29	-0.59	-0.49	-0.30	-0.47	-0.42	-0.42	-0.61	**-0.45**	**0.04**

Table 24: Results of change in pitch angle at leading edge and 15 mm from the tip of the blade acquired with photogrammetry test for DJI Phantom 3 propeller C.

RPM	Take 1	Take 2	Take 3	Take 4	Take 5	Take 6	Take 7	Take 8	Mean	Standard Mean Error
2500	-	-	-	-	-	-	-	-	**-**	**-**
3000	-0.10	-0.16	-0.30	-0.07	-0.19	-0.28	-0.30	-0.25	**-0.21**	**0.03**
3500	-0.10	0.19	-0.28	0.13	0.18	-0.10	-0.04	-0.09	**-0.01**	**0.06**
4000	-0.30	-0.38	-0.40	-0.42	-0.47	-0.27	-0.35	-0.33	**-0.37**	**0.02**
4500	0.25	0.26	-0.16	0.04	0.12	-0.20	-0.05	0.21	**0.06**	**0.06**
5000	-0.04	-0.16	-0.10	0.09	-0.02	-0.02	-0.04	0.01	**-0.04**	**0.03**
5500	-0.02	0.00	-0.17	-0.12	-0.38	-0.21	-0.16	-0.11	**-0.15**	**0.04**
6000	-	-	-	-	-	-	-	-	**-**	**-**
6500	-0.26	-0.24	-0.33	-0.10	-0.16	-0.38	-0.22	0.00	**-0.24**	**0.04**
7000	-0.27	-0.61	-0.53	-0.53	-0.37	-0.35	-0.60	-0.63	**-0.49**	**0.05**
7500	-0.93	-0.52	-0.70	-	-	-	-	-	**-0.72**	**0.12**

Appendix D—Performance Results

During the DSLR camera tests, the performance of the propellers was recorded with a 6-degree-of-freedom load cell. The main interest was the out-of-plane force, which can be an indicator of roughly how much lift is generated for each RPM. This total lift was then used to compare the out-of-plane defection, to see how much a single blades' performance affects the total deflection.

Figure 32 depicts the out-of-plane force as a function of measuring points. The measuring points 1 and 18 are the static points; points 2 and 17 are the housekeeping points at 5300 RPM while points 3 to 16 correspond to the RPM of 2500 to 8500 with a step of 500, respectively. Housekeeping points were added to check if there was any float in the load due to heating up of the load cell. The performance results below are only for run 3 where five DJI Phantom 3 blades were tested and compared.

Figure 33 shows the out-of-plane force as a function of measuring points for the T-motor propeller. Points 1 and 11 are the static points; points 2 and 10 are the housekeeping points at 3300 RPM while points 3 to 9 correspond to the RPM of 2000 to 5000 with a step of 500, respectively.

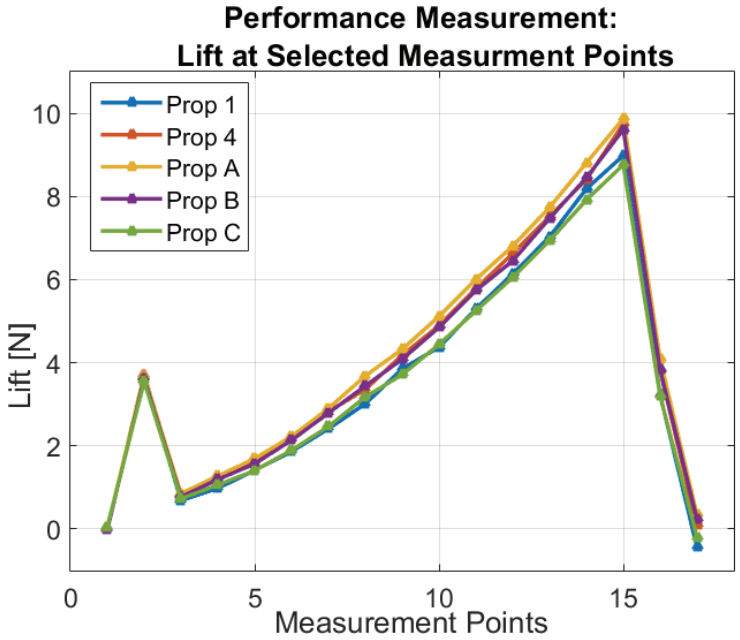

Figure 32: Performance measurements for the five DJI Phantom 3 propellers.

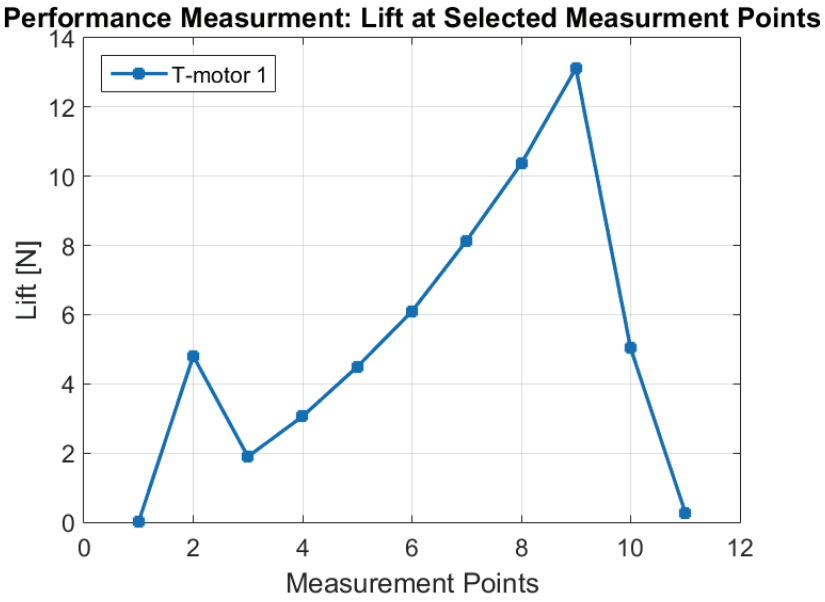

Figure 33: Performance measurements for T-motor 15x5 propeller.